Effect of Terbium in tin antimonide host

By

DEEPIKA. R

(14PPH004)

A dissertation submitted to

Avinashilingam Institute for Home Science and Higher Education for Women University

Coimbatore - 641 043.

In partial fulfilment of the requirements for degree of

Master of Science in Physics

April, 2016

Effect of Terbium in tin antimonide host

By

DEEPIKA. R

(14PPH004)

A dissertation submitted to

Avinashilingam Institute for Home Science and Higher Education for Women University

Coimbatore - 641 043.

In partial fulfilment of the requirements for degree of

Master of Science in Physics

April, 2016

29/4/16

Signature of Head of the Department

29/04/2016

Signature of the Supervisor

ACKNOWLEDGEMENT

I owe my sincere thanks to **Lord Almighty** and **My Lovable Parents** without whom I would have been nothing and showering their generous blessings upon me in all endeavors.

I wish to express my profound sense of gratitude **Shri**, **Dr.P.R.Krishnakumar**, Chancellor, Avinashilingam Institute for Home Science and Higher Education for Women, Coimbatore, for providing the facilities to conduct this study.

I extend my thanks to **Hon.Col.Dr. (Tmt.) Premavathy Vijayan,** M.Sc., M.Ed., Dip. Spl.Edn., M.Phil., Ph.D., Vice Chancellor (i/c), Avinashilingam Institute for Home Science and Higher Education for Women, Coimbatore, for providing flamboyant help towards the completion of the study.

I record my deep sense of gratitude and indebtedness to, **Dr. (Tmt.) A.Venmathi,** M.Sc, Dip.Ed, M.Phil, Ph.D. Registrar (i/c), Avinashilingam Institute for Home Science and Higher Education for Women, Coimbatore, for providing adequate help for the study.

I place on record my heartfelt thanks to **Hon.Col.Dr. (Tmt.) Saroja Prabakaran,** M.A.,Dip.Ed.,Ph.D.,Former Vice Chancellor, The Director, Hall of Residence, Avinashilingam Educational Trust Institutions Hostel, Coimbatore, for extending all possible help towards the completion of the study.

I gratefully record my sincere thanks to **Dr. (Tmt.) A. Parvathi**, M.Sc.,Dip. Ed., M.Phil., Ph.D., Dean, Faculty of Science, Avinashilingam Institute for Home Science and Higher Education for Women, Coimbatore, for timely help rendered throughout the course.

I whole heartily thank **Dr. (Tmt.) J. Shanthi,** M.Sc., M.Phil., Ph.D., Associate Professor and Head of the Department of Physics, Avinashilingam Institute for Home Science and Higher Education for Women, Coimbatore, for her encouragement and generous help which was of great value.

I express my heartiest thanks to my guide **Dr. (Tmt.) B.Nalini,** M.Sc., Ph.D., M.S (Edu.Mgt.), STA Fellow, AIST Fellow (Japan), Assistant Professor, Department of Physics, Avinashilingam Institute for Home Science and Higher Education for Women, Coimbatore, for her inspiring guidance, meticulous care, patience, help, encouragement, motivation, and skillful and expert suggestions in completion of this work.

I sincerely thank all **the staff members** of the Department of Physics, Avinashilingam Institute for Home Science and Higher Education for Women, Coimbatore, for their help and support.

I would like to express my special thanks to **my parents**, **brother**, **sister**, **my friends** and all **my well wishers** for their constant encouragement, support and help in carrying out this work successfully.

DEEPIKA. R

CONTENT

LIST OF FIGURES

LIST OF TABLES

CHAPTER -I

INTRODUCTION

1.1 PHOSPHOR

A phosphor is a substance that exhibits the phenomenon of luminescence. This includes both phosphorescent materials, which show a slow decay in brightness (> 1 ms), and fluorescent materials, where the emission decay takes place over tens of nanoseconds. Phosphorescent materials are known for their use in radar screens and glow-in-the-dark materials, whereas fluorescent materials are common in cathode ray tube (CRT) and plasma video display screens, sensors, and white LEDs.

Phosphors are often transition metal compounds or rare earth compounds of various types. The most common uses of phosphors are in CRT displays and fluorescent lights. Phosphors are used in solid state white lighting to down convert part or all of the blue or UV light emitted from a light emitting diode (LED) into light of longer wavelengths, such as blue, green, yellow or red. The different colors of the visible spectrum mix to create white light. Phosphors are an important component in white LEDs. (1)

1.2 PRINCIPLE

A material can emit light either through incandescence, where all atoms radiate, or by luminescence, where only a small fraction of atoms, called emission centers or luminescence center, emit light. In inorganic phosphors, these homogeneities in the crystal structure are created usually by addition of a trace amount of dopants, impurities called activators. The wavelength emitted by the emission center is dependent on the atom itself and on the surrounding crystal structure.

The scintillation process in inorganic materials is due to the electronic band structure found in the crystals. An incoming particle can excite an electron from the valence band to either the conduction band or the exciton band. This leaves an associated hole behind, in the valence band. Impurities create electronic levels in the forbidden gap. The excitons are loosely bound electron-hole pairs that wander through the crystal lattice

until they are captured as a whole by impurity centers. The latter then rapidly de-excite by emitting scintillation light (fast component). In case of inorganic scintillators, the activator impurities are typically chosen so that the emitted light is in the visible range or near-UV where photomultipliers are effective. The holes associated with electrons in the conduction band are independent from the latter. Those holes and electrons are captured successively by impurity centers exciting certain metastable states not accessible to the excitons. The delayed de-excitation of those metastable impurity states, slowed down by reliance on the low-probability forbidden mechanism.

1.3 PHOSPHOR DEGRADATION

Many phosphors tend to lose efficiency gradually by several mechanisms. The activators can undergo change of valence (usually oxidation), the crystal lattice degrades, atoms often acts as the activators and diffuse through the material, the surface undergoes chemical reactions with the environment with consequent loss of efficiency or buildup of a layer absorbing either the exciting or the radiated energy, etc.

The degradation of electroluminescent devices depends on frequency of driving current, the luminance level, and temperature; moisture impairs phosphor lifetime very noticeably as well. Harder, high-melting, water-insoluble materials display lower tendency to lose luminescence under operation.

1.4 MATERIALS

Phosphors are usually made from a suitable host material with an added activator. The best known type is a copper-activated zinc sulfide and the silver-activated zinc sulfide.

The host materials are typically oxides, nitrides and oxynitrides,[10] sulfides, selenides, halides or silicates of zinc, cadmium, manganese, aluminium, silicon, or various rare earth metals. The activators prolong the emission time (afterglow). In turn, other materials (such as nickel) can be used to quench the afterglow and shorten the decay part of the phosphor emission characteristics.

Many phosphor powders are produced in low-temperature processes, such as sol-gel and usually require post-annealing at temperatures of ~1000 °C, which is undesirable for many applications. However, proper optimization of the growth process allows to avoid the annealing. (2)

Phosphors used for fluorescent lamps require a multi-step production process, with details that vary depending on the particular phosphor. Bulk material must be milled to obtain a desired particle size range, since large particles produce a poor quality lamp coating and small particles produce less light and degrade more quickly. During the firing of the phosphor, process conditions must be controlled to prevent oxidation of the phosphor activators or contamination from the process vessels. After milling the phosphor may be washed to remove minor excess of activator elements. Volatile elements must not be allowed to escape during processing. Lamp manufacturers have changed composition of phosphors to eliminate some toxic elements, such as beryllium, cadmium, or thallium, formerly used. (3)

1.5 APPLICATION

1.5.1 Radioluminescence

Zinc sulfide phosphors are used with radioactive materials, where the phosphor is excited by the alpha- and beta-decaying isotopes, to create luminescent paint for dials of watches and instruments (radium dials). Between 1913 and 1950 radium-228 and radium-226 was used to activate a phosphor made of silver doped zinc sulfide (ZnS:Ag), which give a greenish glow. The phosphor is not suitable to be used in layers thicker than 25 mg/cm², as the self-absorption of the light then becomes a problem. Furthermore, zinc sulfide undergoes degradation of its crystal lattice structure, leading to gradual loss of brightness significantly faster than the depletion of radium. ZnS:Ag coated spinthariscope screens was used by Ernest Rutherford in his experiments discovering atomic nucleus.

Copper doped zinc sulfide (ZnS:Cu) is the most common phosphor used and yields blue-green light. Copper and magnesium doped zinc sulfide (ZnS:Cu,Mg) yields yellow-orange light. Tritium is also used as a source of radiation in various products utilizing tritium illumination.

1.5.2 Electroluminescence

Electroluminescence can be exploited in light sources. Such sources typically emit from a large area, which makes them suitable for backlights of LCD displays. The excitation of the phosphor is usually achieved by application of high-intensity electric field, usually with suitable frequency. Current electroluminescent light sources tend to degrade with use, resulting in their relatively short operation lifetimes.

ZnS:Cu was the first formulation successfully displaying electroluminescence, tested at 1936 by Georges Destriau in Madame Marie Curie laboratories in Paris.

Indium tin oxide composite is used in some Timex watches, though as the electrode material, not as a phosphor itself. "Lighttape" is another trade name of an electroluminescent material, used in electroluminescent light strips

1.5.3 Phosphor thermometry

Phosphor thermometry is a temperature measurement approach that uses the temperature dependence of certain phosphors. For this, a phosphor coating is applied to a surface of interest and, usually, the decay time is the emission parameter that indicates temperature. Because the illumination and detection optics can be situated remotely, the method may be used for moving surfaces such as high speed motor surfaces. Also, phosphor may be applied to the end of an optical fiber as an optical analog of a thermocouple.

1.5.4 Lighting

Phosphor layers provide most of the light produced by fluorescent lamps, and are also used to improve the balance of light produced by metal halide lamps. Various neon signs use phosphor layers to produce different colors of light. Electroluminescent displays found, for example, in aircraft instrument panels, use a phosphor layer to produce glare-free illumination or as numeric and graphic display devices. White LED lamps consist of a blue or ultra-violet emitter with a phosphor coating that emits at longer wavelengths, giving a full spectrum of visible light.

1.5.5 White LEDs

White light-emitting diodes are usually blue InGaN LEDs with a coating of a suitable material. Cerium(III)-doped YAG (YAG:Ce^{3+}, or $Y_3A_{l5}O_{12}$:Ce^{3+}) is often used; it absorbs the light from the blue LED and emits in a broad range from greenish to reddish, with most of output in yellow. This yellow emission combined with the remaining blue emission gives the "white" light, which can be adjusted to color temperature as warm (yellowish) or cold (bluish) white. The pale yellow emission of the Ce^{3+}:YAG can be tuned by substituting the cerium with other rare earth elements such as terbium and gadolinium and can even be further adjusted by substituting some or all of the aluminium in the YAG with gallium. However, this process is not a phosphorescence. The yellow light is produced by a process known as scintillation, the complete absence of an afterglow being one of the characteristics of this process. (4)

ELEMENT INVOLVED IN THIS PROJECT

1.6 TERBIUM

Terbium is a chemical element with symbol Tb and atomic number 65. It is a silvery-white rare earth metal that is malleable, ductile and soft enough to be cut with a knife. Terbium is never found in nature as a free element, but it is contained in many minerals, including cerite, gadolinite, monazite, xenotime and euxenite.

Swedish chemist Carl Gustaf Mosander discovered terbium as a separate elemental compound in 1843. He detected it as an impurity in yttrium oxide, Y_2O_3. Yttrium and terbium are named after the village of Ytterby in Sweden. Terbium was not isolated in pure form until the advent of ion exchange techniques.

Atomic Number: 65

Atomic Weight: 158.92535

Melting Point: 1629 K (1356°C or 2473°F)

Boiling Point: 3503 K (3230°C or 5846°F)

Density: 8.23 grams per cubic centimeter

Phase at Room Temperature: Solid

Element Classification: Metal

Period Number: 6

Group Number: none

Group Name: Lanthanide

Terbium is used to dope calcium fluoride, calcium tungstate and strontium molybdate, materials that are used in solid-state devices, and as a crystal stabilizer of fuel cells which operate at elevated temperatures. As a component of Terfenol-D (an alloy that expands and contracts when exposed to magnetic fields more than any other alloy), terbium is of use in actuators, in naval sonar systems and in sensors.

1.6.1 Physical properties

Terbium is a silvery-white rare earth metal that is malleable, ductile and soft enough to be cut with a knife. It is relatively stable in air as compared to other lanthanides. Terbium exists in two crystal allotropes with a transformation temperature of 1289 °C between them. (5)

The terbium(III) cation is brilliantly fluorescent, in a bright lemon-yellow color that is the result of a strong green emission line in combination with other lines in the orange and red. The yttrofluorite variety of the mineral fluorite owes its creamy-yellow fluorescence in part to terbium. Terbium easily oxidizes, and is therefore used in its elemental form specifically for research. Single Tb atoms have been isolated by implanting them into fullerene molecules. (6)

1.6.2 Chemical properties

Most of the world's terbium supply is used in green phosphors. Terbium oxide is in fluorescent lamps and TV tubes. Terbium green phosphors are combined with divalent europium blue phosphors and trivalent europium red phosphors to provide "trichromatic" lighting technology, a high-efficiency white light used for standard illumination in indoor lighting.

Terbium oxide is used in green phosphors in fluorescent lamps and color TV tubes. Sodium terbium borate is used in solid state devices. The brilliant fluorescence allows terbium to be used as a probe in biochemistry, where it somewhat resembles calcium in its behavior. Terbium "green" phosphors (which fluoresce a brilliant lemon-yellow) are combined with divalent europium blue phosphors and trivalent europium red phosphors to provide the "trichromatic" lighting technology which is by far the largest consumer of the world's terbium supply. Trichromatic lighting provides much higher light output for a given amount of electrical energy than does incandescent lighting. (5)

1.6.3 Sources of terbium

Along with other rare earth elements, terbium can be found in minerals, including cerite and gadolinite. The element can be extracted from monazite, in which it is present to the extent of 0.03 percent; from euxenite, a complex oxide containing 1 percent or more of terbia; and xenotime.

Recent advances ion-exchange techniques for separating the rare earth elements have enabled the isolation of terbium. One method for producing the rare earth metal is by reducing the anhydrous chloride or fluoride with calcium, although other methods of isolation are available. Vacuum remelting can remove calcium and tantalum impurities.

1.6.4 Uses of terbium

Terbium is used to dope calcium fluoride, calcium tungstate and strontium molybdate, all used in solid-state devices. It is also used in low-energy light bulbs and mercury lamps. It has been used to improve the safety of medical x-rays by allowing the same quality image to be produced with a much shorter exposure time. Terbium salts are used in laser devices.

An alloy of terbium, dysprosium and iron lengthens and shortens in a magnetic field. This effect forms the basis of loudspeakers that sit on a flat surface, such as a window pane, which then acts as the speaker.

1.6.5 Occurrence in nature

Terbium is one of the rarest of the Lanthanides. It ranks about 55th among the elements in the Earth's crust. It is about as abundant as molybdenum and tungsten, but more abundant than iodine, silver, and gold. Terbium occurs with other Lanthanides in minerals such as monazite, cerite, gadolinite, xenotime, and euxenite. (7)

1.7 ANTIMONY

A lustrous gray metalloid, it is found in nature mainly as the sulfide mineral stibnite (Sb_2S_3). Antimony compounds have been known since ancient times and were used for cosmetics; metallic antimony was also known, but it was erroneously identified as lead upon its discovery. In the West, it was first isolated by Vannoccio Biringuccio and described in 1540, although in primitive cultures its powder has been used to cure eye ailments, as also for eye shadow, since time immemorial, and is often referred to by its Arabic name, kohl. The industrial methods to produce antimony are roasting and reduction using carbon or direct reduction of stibnite with iron. (8)

Atomic Number: 51

Atomic Weight: 121.760

Melting Point: 903.78 K (630.63°C or 1167.13°F)

Boiling Point: 1860 K (1587°C or 2889°F)

Density: 6.685 grams per cubic centimeter

Phase at Room Temperature: Solid

Element Classification: Semi-metal

Period Number: 5

Group Name: Pnictogen

1.7.1 Characteristics:

Antimony is metalloid, so it has some metallic properties but not enough to be classified as a true metal. Physically, it behaves like sulfur while chemically it is more

metallic. Antimony's electrical and thermal conductivity are lower than most metals' conductivities. Antimony is a brittle, fusible, crystalline solid. It is easily powdered. Antimony also has the unusual property that (like water) it expands as it freezes. Four other elements expand when they freeze; silicon, bismuth, gallium and germanium. In addition to the usual form of antimony, there are two allotropes: yellow crystalline and amorphous black. (9)

1.7.2 Uses of antimony

The major use of antimony is in lead alloys - mainly for use in batteries - adding hardness and smoothness of finish. The higher the proportion of antimony in the alloy, the harder and more brittle it will be. Alloys made with antimony expand on cooling, retaining the finer details of molds. Antimony alloys are therefore used in making typefaces for clear, sharp printing. Babbit metals, used for machinery bearings, are alloys of lead, tin, copper and antimony. These metals are hard but slippery and so ideal for use as bearings. Antimony is used in the semiconductor industry as an n-type dopant for silicon. Antimony trioxide is used as a flame retardant in adhesives, plastics, rubber and textiles. (10)

1.7.3 Occurrence in nature

Antimony is rarely found in its native (as an element) state. Instead, it usually occurs as a compound. The most common minerals of antimony are stibnite, tetrahedrite, bournonite, boulangerite, and jamesonite. In most of these minerals, antimony is combined with sulfur to produce some form of antimony sulfide (Sb_2S_3). The largest producers of antimony are China, Russia, Bolivia, South Africa, and Kyrgyzstan, in that order. The United States produces antimony as a by-product at only one silver mine in Idaho. The abundance of antimony is estimated to be about 0.2 parts per million, placing it in the bottom fifth among the chemical elements found in the Earth's crust. It is more abundant than silver or mercury, but less abundant than iodine.

1.8 TIN

Tin is a chemical element with the symbol Sn (for Latin: *stannum*) and atomic number 50. It is a main group metal in group 14 of the periodic table. Tin shows a chemical similarity to neighboring group-14 elements, germanium and lead, and has two possible oxidation states, +2 and the slightly more stable +4. Tin is the 49th most abundant element and has, with 10 stable isotopes, the largest number of stable isotopes in the periodic table. It is a silvery, malleable other metal that is not easily oxidized in air, obtained chiefly from the mineral cassiterite where it occurs as tin dioxide, SnO_2. (11)

Atomic Number: 50

Atomic Mass: 118.71 amu

Melting Point: 231.9 °C (505.05 K, 449.41998 °F)

Boiling Point: 2270.0 °C (2543.15 K, 4118.0 °F)

Number of Protons/Electrons: 50

Number of Neutrons: 69

Classification: Other Metals

Crystal Structure: Tetragonal

Density @ 293 K: 7.31 g/cm3

Color: white

1.8.1 Characteristics:

Tin is a silvery-white, soft, malleable metal that can be highly polished. Tin has a highly crystalline structure and when a tin bar is bent, a 'tin cry' is heard, due to the breaking of these crystals. In compounds tin is usually in the divalent state (Sn^{2+}) or tetravalent state (Sn^{4+}).It resists oxygen and water but dissolves in acids and bases. Exposed surfaces form an oxide film. When heated in air, tin forms tin(IV) oxide (stannic oxide) which is feebly acidic. Tin has two allotropic forms at normal pressure, gray tin and white tin. Pure white tin slowly tends to become the gray powder (gray tin), a change commonly called 'tin pest' at temperatures below 13.2 ^{o}C. Gray tin has no metallic

properties at all. Commercial quality tins are resistant to tin pest as a result of the inhibiting effects of minor impurities.

1.8.2 Uses of Tin

Tin is used as a coating on the surface of other metals to prevent corrosion. 'Tin' cans, for example, are made of tin-coated steel. Tin can is rolled into thin foil sheets (tinfoil). Present day 'tinfoil' to cover or wrap food is usually made from aluminum. Alloys of tin are commercially important in, for example, soft solder, pewter, bronze and phosphor bronze. Tin chloride (stannous chloride, $SnCl_2$) is used as a mordant in dyeing textiles and for increasing the weight of silk. Stannous fluoride (SnF_2) is used in some toothpastes.

1.8.3 Occurrence in nature

Tin is not very abundant in nature. It ranks about 50th on the list of elements most commonly found in the Earth's crust. Estimates are that the crust contains about 1 to 2 parts per million of tin.

By far the most common ore of tin is cassiterite, a form of tin oxide (SnO_2). An ore is a compound or mixture from which an element can be extracted for commercial profit. Cassiterite has been mined for thousands of years as a source of tin. During ancient times, Europe obtained most of its tin from the British Isles. Today, the major producers of tin are China, Indonesia, Peru, Brazil, and Bolivia. The United States produces almost no tin of its own although it is the major consumer of the metal. (12)

REFERENCE

1. Emsley, John (2000). The Shocking History of Phosphorus. London: Macmillan. ISBN 0-330-39005-8.
2. Li, Hui-Li; Hirosaki, Naoto; Xie, Rong-Jun; Suehiro, Takayuki; Mitomo, Mamoru (2007). Adv. Mater. **8** (7–8): 601.
3. Bizarri, G; Moine, B (2005). "On phosphor degradation mechanism: thermal treatment effects". Journal of Luminescence 113 (3–4): 199. Bibcode:2005JLum..113..199B. doi:10.1016/j.jlumin.2004.09.119
4. Youn-Gon Park; et al. "Luminescence and temperature dependency of β-SiAlON phosphor". Samsung Electro Mechanics Co.
5. Jackson, M. (2000). "Magnetism of Rare Earth" (PDF). The IRM quarterly 10 (3)
6. Shimada, T.; Ohno, Y.; Okazaki, T.; et al. (2004). "Transport properties of C78, C90 and Dy@C82 fullerenes - nanopeapods by field effect transistors". Physica E: Low-dimensional Systems and Nanostructures 21 (2–4): 1089–1092.
7. http://www.chemistryexplained.com/elements/P-T/Terbium.html
8. Wang, Chung Wu (1919). "The Chemistry of Antimony". Antimony: Its History, Chemistry, Mineralogy, Geology, Metallurgy, Uses, Preparation, Analysis, Production and Valuation with Complete Bibliographies (PDF). London, United Kingdom: Charles Geiffin and Co. Ltd. pp. 6–33.
9. Robert E. Krebs, The history and use of our earth's chemical elements: a reference guide., (2006) p219. Greenwood Publishing Group.
10. file:///D:/thesis/ref/Antimony%20%20Uses,%20Pictures,%20Characteristics,%20Properties,%20Periodic%20Table.htm.
11. Jo, Yun Hwan; Jung, Inyu; Choi, Chung Seok; Kim, Inyoung; Lee, Hyuck Mo (2011). "Synthesis and characterization of low temperature Sn nanoparticles for the fabrication of highly conductive ink". Nanotechnology 22 (22): 225701.
12. http://www.chemicool.com/elements/tin.html

CHAPTER-II
REVIEW OF LITERATURE

[1] Ming shyong tsai *et al.*, (2008) modified solid-state reaction method for the formation of terbium aluminum garnet (TAG:Ce) powder was studied. The starting materials, which included terbium oxide (Tb_4O_7), boehmite and cerium chloride ($CeCl_3 \cdot 7H_2O$), were pre-aged at pH 3. This pre-aging process helps to form the core–shell structure, which leads to the formation of TAG:Ce phosphor powder via a solid-state reaction more easily. The emission intensity at 551 nm of the product pre-aged at pH 3 is higher than that formed without pre-aging.

[2] Jyh Ming wu (2008) Sb doped SnO_2 (SnO_2:Sb) nanowires (NWs) were synthesized by thermal evaporation at 900 °C. Thin-film X-ray diffraction showed that as-synthesized nanowires were a single-phase rutile structure. Field emission scanning microscopy revealed that the nanowires had diameters of 80–120 nm and lengths of up to several hundred microns long. High-resolution transmission electron microscopy (HRTEM), electron energy-loss spectroscopy (EELS), and an energy-filtering system were employed to map two-dimensional element concentration. HRTEM images further confirmed that the crystallinity of the nanowires was accompanied by crystal defects with lattice distortion as Sb was incorporated into a SnO_2 nanowire. Cathodoluminescence (CL) spectrophotometer analysis has revealed blue and green emission peaks in both SnO_2:Sb and pure SnO_2 nanowires. The electron field emission values of the SnO_2:Sb and SnO_2 nanowires in the turn-on fields were estimated as ~ 4.9 and 6.5 V/μm, respectively; the current density was 1 $\mu A/cm^2$.

[3] Jing wang *et al.*, (2009) synthesized a novel green phosphor, $Ca_{10}K(PO_4)_7$:Eu^{2+},Tb^{3+},K^+, by high temperature solid-state reaction. The photoluminescence properties showed an efficient energy transfer from Eu^{2+} to Tb^{3+} , where Eu^{2+} ions exhibit a strong excitation band between 350 and 420 nm, matching well with the dominant emission band of (n)-UV (390–420 nm) LED, and Tb^{3+} ions give an intense green emitting light. A green LED with CIE chromaticity coordinates (x = 0.283,

y = 0.383) were fabricated by coating the $Ca_{10}K(PO_4)_7:Eu^{2+},Tb^{3+},K^+$ phosphor onto (n)-UV chip emitting at 398 nm. These results demonstrate that Tb^{3+} ion with low 4f–4f absorption efficiency in (n)-UV region can play a role of activator in narrow green emitting phosphor potentially useful in (n)-UV GaN-based LED through efficient energy feeding by allowed 4f–5d absorption of Eu^{2+} with high oscillator strength.

[4] Te-Wen Kuo *et al.,* (2010) investigated the spectroscopic properties in UV-excitable range for the phosphors of $Sr_3La_2(BO_3)_4:RE^{3+}$ (RE^{3+}=Eu^{3+}, Ce^{3+}, Tb^{3+}). The phosphors were synthesized by conventional solid-state reactions. The photoluminescence (PL) spectra and commission international de I'Eclairage (CIE) coordinates of $Sr_3La_2(BO_3)_4:RE^{3+}$ were investigated. The f–d transitions of Eu^{3+}, Ce^{3+} and Tb^{3+} in the host lattices were assumed and corroborated. The PL and PL excitation (PLE) spectra indicate that the main emission wavelength of $Sr_3La_2(BO_3)_4:Eu^{3+}$ is 611 nm, and $Sr_3La_2(BO_3)_4:Ce^{3+}$ shows dominating emission peak at 425 nm, while $Sr_3La_2(BO_3)_4:Tb^{3+}$ displays green emission at 487, 542, 582 and 620 nm. These phosphors were prepared by simple solid-state reaction at 1000 °C. There are lower reactive temperature and more convenient than commercial phosphors. The $Sr_3La_2(BO_3)_4:Tb^{3+}$ applied to cold cathode fluorescent lamp was found to emit green light and have a major peak wavelength at around 542 nm. These phosphors may provide a new kind of luminescent materials under ultraviolet excitation.

[5] Ayano Toda *et al.,* (2010) reported the luminescence property of a new phosphate phosphor, $RbPO_3$:Tb. A single phase sample was obtained by thermal decomposition of a raw material mixture (RbH_2PO_4 and Tb_4O_7) at 973 K. The phosphor was excited by the UV light, yielding an intense green emission around 550 nm. An intense green emission was originated from the f–f transition of Tb^{3+} ion.

[6] Audrey Potdevin *et al.,* (2010) prepared luminescent Tb^{3+} yttrium-based garnets powders by the sol–gel route. Optical properties of samples have been studied. Excitation spectra have revealed several excitation bands between 200 and 500 nm, which match very well with newly developed AlGaN-based deep-ultraviolet (DUV) or near-UV LEDs.

Excitation profiles were dependent on the matrix formula. Emission spectral features studied upon different UV excitation wavelength have revealed that luminescence efficiency can be significantly improved by tuning the matrix composition. Thus, optical properties can be tuned to optimize the lighting source features, according to the kind of UV LEDs employed.

[7] **Yu Muto *et al.*, (2011)** SnO_2 films doped with Sb (ATO) were deposited both on unheated glass substrates and on glass substrates that had been heated at 200 °C by reactive sputtering of an Sb–Sn alloy target with a plasma control unit (PCU) and mid-frequency (mf, 50 kHz) unipolar pulsing. The PCU feedback system monitors the oxidation states of target surface by detecting the sputtering cathode voltage (impedance control method). The mf pulse wave is approximately square-shaped; this helps to reduce arcing on the target when high power density is applied on the cathode. In case of the ATO depositions on the heated substrate at 200 °C in the "transition region" of reactive sputtering, the deposition rate was 280 nm/min, the lowest resistivity of the ATO films was 4.6×10^{-3} Ω cm and the optical transmittance was over 80% in the visible region of light.

[8] **Dimple P. Dutta *et al.*, (2011**) synthesized undoped CeO_2, and single and triple doped CeO_2:M (where M=Dy^{3+}, $Tb^{3+}$and Eu^{3+}) nanophosphors through a simple sonochemical process and characterized by using X-ray diffraction (XRD), scanning electron microscopy (SEM), transmission electron microscopy (TEM), high resolution transmission electron microscopy (HRTEM), EDS and photoluminescence (PL) spectrophotometry. The TEM micrographs show that resultant nanoparticles have flower-like shape. The doped samples showed multicolor emission on single wavelength excitation. Energy transfer was observed from host to the dopant ions. Characteristic blue emission from Dy^{3+} ions, green from Tb^{3+} ions and red from Eu^{3+} ions were observed. The CIE coordinates of the triple doped $Ce_{0.86}Dy_{0.005}Tb_{0.055}Eu_{0.08}O_2$ nanoflowers lie in the white light region of the chromaticity diagram.

[9] Feng dan wu *et al.*, (2011) Antimony-doped tin oxide (ATO) nanotubes were synthesized by a modified template method. The nanotubes, which were ~ 200 nm in diameter and 10–20 nm in wall thickness, were composed of a large number of 5–15 nm ATO nanocrystals. The doping level of Sb in the ATO could be varied by the experimental conditions. ATO nanotubes with Sn:Sb ratios of 9:1 or 5:1, in particular, were good reversible Li storage materials, showing high capacities and good cyclability at both common and high rates of charge and discharge.

[10] B.V. Ratnam *et al.*, (2013) synthesized an efficient green emitting Tb^{3+} doped $NaCaPO_4$ (NCP) phosphor by using conventional solid-state reaction for solid-state lighting applications. X-ray diffraction (XRD), field emission scanning electron microscope (FE-SEM), FT-IR, emission and excitation properties were extensively investigated for NCP phosphors. X-ray diffraction analysis confirmed the formation of $NaCaPO_4$ with orthorhombic structure. The excitation spectrum consists of strong 4f–4f transition at around 370 nm, which has higher intensity than the f–d transition. Emission spectra indicated that this phosphor can be efficiently excited by UV light in the range from 250 to 400 nm, and shows strong emission band centered at 547 nm. Analysis of the emission spectra with different Tb^{3+} concentrations revealed that the optimum dopant concentration for these NCP phosphors was about 5 mol% of Tb^{3+}. Diminishing of $^5D_3$ level and increasing of $^5D_4$ level emission intensity with the Tb^{3+} concentration explained successfully. The emission color was analyzed and confirmed with the help of chromaticity coordinates and color temperature. The excellent luminescent properties of $NaCaPO_4$:Tb^{3+} phosphor makes it as a potential green phosphor upon near-UV LED excitation.

[11] S.J. Yoon *et al.*, (2014) synthesized Tb^{3+}-doped $La_{1-x}AlO_3$ phosphor powders by the solution combustion method, using citric acid as the combustion fuel. The crystal structure and photoluminescence properties of $La_{1-x}AlO_3$:xTb^{3+} phosphors were studied, depending on Tb^{3+} content. The strongest emission peak was found at 543 nm, which originates from the $^5D_4 \rightarrow {}^7F_5$ transition of Tb^{3+} ions, indicating green emission. Among the fabricated phosphors, the $La_{0.9}AlO_3$:$0.1Tb^{3+}$ phosphor emits the strongest green light.

The excellent luminescent properties make it a possible candidate for white light-emitting diodes and various photonic applications.

[12] Vinod Kumar *et al*., (2014) synthesised Terbium doped Zinc oxide ($ZnO:Tb^{3+}$) nano-phosphors (NPr) with a hexagonal wurtzite structure by a solution combustion method. X-ray photoelectron spectroscopy confirmed the formation of different kind of defects for the undoped and lower Tb doping concentrations and the formation of Tb_2O_3 at higher doping concentrations. A broadband orange-red emission ranging from 500 to 850 nm was obtained from the undoped ZnO while white light emission was observed from ZnO doped with 5 mol% of Tb. The colour of the emission of the $ZnO:Tb3^+$ NPr was tuned by varying the concentrations of Tb^{3+} in the ZnO host. The $ZnO:Tb^{3+}$ NPr have potential applications in solid state lighting.

[13] Jianyin zhang *et al.*, (2014) Porous Sn/SnSb negative electrodes for lithium ion batteries were directly prepared by electro-reduction of the SnO_2–Sb_2O_3 (molar ratio = 4:1) composite electrodes in 1 mol/L H_2SO_4. After the reduction, the original dense SnO_2–Sb_2O_3 composite electrode changed into a porous structure with the oxides almost completely reduced to nanoparticles of Sn and SnSb alloy. As the precursor electrode showed very poor electrochemical performances in lithium ion batteries, the resultant metallic porous Sn/SnSb electrode exhibited high charge capacity (800 mAh/g) and good cycling stability (70% of capacity retention at the 40th cycle) between 0.02 and 1.5 V (vs. Li/Li^+) at a current density of 100 mA/g. More porous Sn/SnSb electrode was derived from the SnO_2–Sb_2O_3 composite precursor using pore-forming by NH_4HCO_3 (15 vol.%), showing enhanced electrochemical performances with an initial capacity of 900 mAh/g at 100 mA/g, and 520 mAh/g at 1 A/g at the 40th charging–discharging cycle.

[14] Anxiang Wang, et al., (2014) the vapor liquid phase equilibrium of Sn-Sb alloy was calculatedby the molecular interaction volume model (MIVM), which was used to predict the element distribution of Sn-Sb alloy between vapor and liquid phase during vacuum distillation. In this central composite design (CCD) was used to optimize the process parameters influencing the content of Sn in liquid phase and the direct yield of Sn.

Distillation temperature, feeding materials and soaking time are the studied parameters.Two quadratic mathematical model equations were derived for predicting the content of Sn in liquid phase and the direct yield of Sn. The analysis of variance (ANOVA) shown that distillation temperature was the most significantfactor affecting the separation of Sn-Sb alloy. In the process optimization, while the direct yield of Sn equal to 92%, the maximum content of Sn in liquid phase should be 99.66 wt.% under the conditions of 1531 K, 137 g and 46 min. The confirmation test values of 91.22% and 99.43 wt.% were fair agreement with the predicted data, which demonstrated that these models were very good and can be used for parameter optimization in vacuum distillation.

[15] Lichao Zhang, et al., (2014) a new type of Ti/SnO2-Sb electrode modified with carbon nanotube (CNT) has been fabricated using apulse electrode position method. The electrode modified with CNT versus without CNT has larger surface area and smaller crystallite particles (41.9 nm versus 46.8 nm) as seen by scanning electron microscopy(SEM), and calculated through X-ray diffraction (XRD), respectively. It means that the CNT-modified elec-trode can provide more active sites for electrochemical oxidation of organic pollutants. Oxygen evolution potential of the CNT-modified electrode has 0.07 V higher over potential in the Linear sweep voltammetry(LSV) curve. The service lifetime of Ti/SnO2-Sb-CNT electrode is 4.8 times longer than that of the Ti/SnO2-Sb electrode without CNT modifying. The Ti/SnO2-Sb-CNT electrode is demonstrated to have a superior electrochemical oxidation and degradation abilities using Acid Red 73 (AR 73) as a model organic pollute-ant. The CNT-modified electrode has higher kinetic rate constant, chemical oxygen demand (COD) and total organic carbon (TOC) removals, and mineralization current efficiency, which is 1.93, 1.27, 1.26, and1.38 times those of the Ti/SnO2-Sb electrode, respectively. The repeated experiments prove the repro-ducibility of the data. Ti/SnO2-Sb-CNT electrode is 1.15 times more effective in permeation flux than the Ti/SnO2-Sb electrode when combining electro-catalytic oxidation and nano filtration for treating dye wastewater.

[16] K. Munirathnam *et al*., (2015) prepared alkaline phosphate based $LiNa_3P_2O_7:Tb^{3+}$ phosphors by solid state reaction method. X-ray diffraction (XRD) analysis shows that all the powders possess orthorhombic structure. Fourier transform infrared (FTIR) spectroscopy studies suggest that the phosphor belong to the diphosphate family. The morphology of the phosphors is identified by scanning electron microscopy (SEM). Upon 378 nm excitation, the $LiNa_3P_2O_7:Tb^{3+}$ phosphors shown emission bands at 482, 545, 588 and 620 nm corresponding to the transitions $^5D_4 \rightarrow {}^7F_6$, $^5D_4 \rightarrow {}^7F_5$, $^5D_4 \rightarrow {}^7F_4$ and $^5D_4 \rightarrow {}^7F_3$, respectively. The optimized concentration of Tb^{3+} in $LiNa_3P_2O_7$ phosphor was found to be 9 mol%. The concentration quenching mechanism was proved to be the exchange interaction between two nearest Tb^{3+} ions with the critical distance (R_c) of 1.18 nm. The Commission International de l'Eclairage (CIE) coordinates evidence that the phosphors emit in the green light region. Thermoluminescence properties of the prepared phosphors were studied by pre-irradiating the powders with different doses of UV irradiation. The kinetic parameters of TL glow curves were calculated using Chen's peak shape method.

[17]Laxmikanta Dua *et al*.,(2016) Sol–gel Mn(II) doped antimony tin oxide films were developed with precursor of atomic ratio range, Sn:Sb:Mn = 68–72:23–25:9–3. The X-ray diffraction patterns depict tetragonal cassiterite phase of SnO_2. Transmission electron microscopy images suggest the nanostructured form of the doped materials. The increase in crystallite size with Mn(II) concentration is reflected by the larger band gap values (4.61–4.73 eV) arising from the excitonic transitions which also respond to PL emissions. Hall effect measurements show that the carrier concentration increases but mobility decreases for Mn(II) doping. Room temperature ferromagnetism with different saturation magnetic moments (M_s) has been observed for all dopant concentrations, 3–9 at%.

[18] L.X. Lovisa *et al*., (2016) investigated the emission spectrum of the particles in the red, green, and blue regions under UV excitation. The search for high efficiency, reliable, low power consumption and environmental friendly materials for white light-emitting diodes has become a proficient field. Single-phase doped materials have been made to solve some of these challenges. Particles with color-tunable emission can be obtained by a combination of some lanthanide ions in the host material. The luminescence properties and crystalline structure of ZrO_2 particles co-doped with rare earth ions ($RE^{3+} = Tb^{3+}$,

Eu^{3+} and Tm^{3+}) calcined at different temperatures were studied. The x and y coordination chromaticity - (x = 0.34, y = 0.34) and (x = 0.31, y = 0.34) - presented values close to those of the white color (x = y = 0.33). The ZrO_2:RE^{3+} powers were successfully obtained by the complex polymerization method.

[19] Yanyan Cao *et al.*, (2016) synthesized a series of Eu^{2+}/Mn^{2+}/Tb^{3+} doped $LiSrPO_4$ phosphors by the solid state reaction. The XRD results show that all phosphors have the pure hexagonal crystal structure, indicating the doping ions have no influence on the phase of $LiSrPO_4$ host. Under the excitation at 365 nm, $LiSrPO_4$/Eu^{2+} phosphors emit blue emission originating from the $4f^65d^1 \rightarrow 4f^7$ transitions of Eu^{2+}. The Eu^{2+}/Mn^{2+} or Tb^{3+} codoped $LiSrPO_4$ phosphors show not only the emission of Eu^{2+} but also the red emission coming from the $^4T_2 \rightarrow {}^6A_{1g}$ transitions of Mn^{2+} or green emissions induced by the $^5D_4 \rightarrow {}^7F_j$ transitions of Tb^{3+}. The increasing Mn^{2+} or Tb^{3+} concentration induces the decrease of Eu^{2+} emission intensity, which suggests the energy from Eu^{2+} to Mn^{2+} or Tb^{3+} in $LiSrPO_4$ host. For $LiSrPO_4$:7 mol%Eu^{2+}/5 mol%Mn^{2+}/5 mol%Tb^{3+} phosphor, the white light can be obtained under the 365 nm excitation.

[20] K. Park *et al.*, (2016) prepared Eu^{3+}-and Tb^{3+}-doped $YAlO_3$ phosphors by solid-state reaction method and their photoluminescence properties were investigated as functions of the $Eu^{3+}$and Tb^{3+}concentrations. The phosphors crystallize in the orthorhombic crystal structure. Under near-ultraviolet excitation (398 nm), the emission spectra of $Y_{1-x}AlO_3$:xEu^{3+}($0.02 \leq x \leq 0.1$) phosphors show several strong peaks at 593, 616, 655, and 697 nm, which were attributed to the $^5D_0 \rightarrow {}^7F_J$ (J=1, 2, 3, and 4) transitions of Eu^{3+}ions. A high value of $(^5D_0 \rightarrow {}^7F_2)/(^5D_0 \rightarrow {}^7F_1)$ is obtained for the $Y_{1-x}AlO_3$:xEu^{3+}phosphors, indicative of high-purity red emission. Furthermore, the emission peaks of $Y_{1-y}AlO_3$:yTb^{3+}($0.04 \leq y \leq 0.2$) phosphors were detected at 489, 544, 585, and 621 nm, which were due to the $^5D_4 \rightarrow {}^7F_6$, $^5D_4 \rightarrow {}^7F_5$, $^5D_4 \rightarrow {}^7F_4$, and $^5D_4 \rightarrow {}^7F_3$ transitions of the Tb^{3+}ions, respectively. The emission peak (544 nm) corresponding to the $^5D_4 \rightarrow {}^7F_5$ transition is the most intense, which is advantageous for high green color purity. White light can be obtained by combining blue GaN LED chips with the red $Y_{1-x}AlO_3$:$xEu^{3+}$and green $Y_{1-y}AlO_3$:yTb^3 phosphors prepared.

REFERENCE

1. Ming-Shyong Tsai, Guang-Mau Liu, Shyan-Lung Chung**,** Fabrication of cerium active terbium aluminum garnet (TAG:Ce) phosphor powder via the solid-state reaction method**,** Materials Research Bulletin, Volume 43, Issue 5, 6 May 2008, Pages 1218–1222

2. Jyh ming wu, Characterizing and comparing the cathodoluminesence and field emission properties of Sb doped SnO_2 and SnO_2 nanowires, thin solid film volume 517, Issue 3, December 2008, pages:1289-129

3. Jing Wang, Zhiyang Zhang, Mei Zhang, Qiuhong Zhang, Qiang Su, Jinke Tang**,** The energy transfer from Eu^{2+} to Tb^{3+} in $Ca_{10}K(PO_4)_7$ and its application in green light emitting diode**,** Journal of Alloys and Compounds, Volume 488, Issue 2, 4 December 2009, Pages 582–585

4. Te-Wen Kuo' , Teng-Ming Chen**,** Synthesis and luminescence properties of Eu^{3+}, Ce^{3+} and Tb^{3+}-activated $Sr_3La_2(BO_3)_4$ under UV excitation**,** Journal of Luminescence, Volume 130, Issue 3, March 2010, Pages 483–487

5. Ayano Toda, Kazuyoshi Uematsu, Tadashi Ishigaki, Kenji Toda, Mineo Sato, Synthesis and luminescence property of new phosphate phosphor, $RbPO_3$:Tb, Materials Science and Engineering: B, Volume 173, Issues 1–3, 15 October 2010, Pages 168–170

6. Audrey Potdevin, Geneviève Chadeyron, Rachid Mahiou**,** Tb^{3+}-doped yttrium garnets: Promising tunable green phosphors for solid-state lighting**,** Chemical Physics Letters, Volume 490, Issues 1–3, 16 April 2010, Pages 50–53

7. Yu Muto, Nobuto Oka, Naoki Tsukamoto, Yoshinori Iwabuchi, Hidefumi Kotsubo, Yuzo Shigesato, High-rate deposition of Sb-doped SnO_2 films by reactive sputtering using the impedance control method, Thin Solid Films, Volume 520, Issue 4, 1 December 2011, Pages: 1165-1366

8. Dimple P. Dutta, N. Manoj, A.K. Tyagi, White light emission from sonochemically synthesized rare earth doped ceria nanophosphors, Journal of Luminescence, Volume 131, Issue 8, August 2011, Pages 1807–1812

9. Feng dan wu, minghong wu, youg wang, Antimony-doped tin oxide nanotubes for high capacity lithium storage, Electrochemistry communications, volume 13, Issue 5 may 2011, Pages :433-436

10. B.V. Ratnam, M. Jayasimhadri, G. Bhaskar Kumar, Kiwan Jang, S.S. Kim, Y.I. Lee, J.M. Lim, D.S. Shin, T.K. Song, Synthesis and luminescent features of $NaCaPO_4:Tb^{3+}$ green phosphor for near UV-based LEDs, Journal of Alloys and Compounds, Volume 564, 5 July 2013, Pages 100–104
11. S.J. Yoon, S.J. Dhoble, K. Park, Synthesis and photoluminescence properties of $La_{1-x}AlO_3:xTb^{3+}$ green phosphors for white LEDs, Ceramics International, Volume 40, Issue 3, April 2014, Pages 4345–4350
12. Vinod Kumar, H.C. Swart, Mukut Gohain, Vijay Kumar, S. Som, B.C.B. Bezuindenhoudt, O.M. Ntwaeaborwa, Influence of ultrasonication times on the tunable colour emission of ZnO nanophosphors for lighting applications**,** Ultrasonics Sonochemistry, Volume 21, Issue 4, July 2014, Pages 1549–1556
13. Jianyin zhang, zhong wang, yanzhong hong, shengxianli, xianbo jin, Electrochemical fabrication of porous Sn/SnSb negative electrodes from mixed SnO_2–Sb_2O_3, electrochemistry comminucation, volume 38 , January 2014, pages:36-39
14. Anxiang Wang , Yifu Li , Bin Yang , Baoqiang Xu , Lingxin Kong , Dachun Liu , Process optimization for vacuum distillation of Sn-Sb alloy by response surface methodology, Volume 109 20 November 2014, pages:127-134.
15. Lichao Zhang, Li Xua, Jing He, Jiejing Zhang, Preparation of Ti/SnO2-Sb electrodes modified by carbon nanotube for anodic oxidation of dye wastewater and combination with nanofiltration, Electrochimica Acta, volume 117, 20 January 2014, pages :192– 201.
16. K. Munirathnam, G.R. Dillip , B. Ramesh, S.W. Joo , B. Deva Prasad Raju**,** Synthesis, photoluminescence and thermoluminescence properties of $LiNa_3P_2O_7:Tb^{3+}$ green emitting phosphor**,** Journal of Physics and Chemistry of Solids, Volume 86, November 2015, Pages 170–176
17. Laxmikanta Dua, Prasanta K. Biswas, Synthesis and characterization of nanostructured Mn(II) doped antimony-tin oxide (ATO) films on glass, Applied Surface Science, Volume 379, (30 August 2016)
18. L.X. Lovisa, V.D. Araújo, R.L. Tranquilin, E. Longo, M.S. Li, C.A. Paskocimas, M.R.D. Bomio, F.V. Motta, White photoluminescence emission from ZrO_2 co-doped with Eu^{3+}, Tb^{3+} and Tm^{3+}, Journal of Alloys and Compounds, Volume 674, 25 July 2016, Pages 245–251

19. Yanyan Cao, Naidi Liu, Jie Tian, Xiao Zhang, Solid state synthesis and tunable luminescence of $LiSrPO_4:Eu^{2+}/Mn^{2+}/Tb^{3+}$ phosphors, Polyhedron, Volume 107, 9 March 2016, Pages 78–82
20. K. Park, H. Kim, D.A. Hakeem, Photoluminescence properties of Eu^{3+}-and Tb^{3+}-doped $YAlO_3$ phosphors for white LED applications, Ceramics International, Volume 42, Issue 8, June 2016, Pages 10526–10530

CHAPTER- III

MATERIALS AND METHODS

3.1 INTRODUCTION

This chapter describes experimental techniques used in the preparation and characterization on earth element Tb (terbium). It is the most rare earth metal. In this study sol- gel technique used to method of preparation. The various experimental techniques such as X-ray Diffraction (XRD), Photo luminescence (PL), and Fourier Transform Infrared Spectroscopy (FTIR), UV (Ultra-violet) spectrum studies have been employed to understand the details of phase, functional group and optical structure of the sample was analyzed in each techniques.

3.1.1 Raw Materials Methods

There are four raw materials used in solution A:

- Tin chloride ($Sncl_2$)
- Antimony chloride ($Sbcl_3$)
- Tri sodium citrate($Na_3C_6H_5O_7$)
- Terbium chloride(Tb)

The raw materials have chosen (2:3) in appropriate gram molecular weights and dissolved in 50 ml distilled water. The solution is stirred for 30min.

There are two raw materials used in solution B

- Sodium hydroxide (NaOH)
- Sodium borohydride ($NaBH_4$)

Sodium hydroxide (NaOH) and Sodium borohydride ($NaBH_4$) are taken in appropriate gram molecular weights and dissolved in 40ml distilled water. This solution is stirred for 20min.

3.1.2 Experimental Details

There are six steps involved in the preparation,namely;

Step 1: After the solution A and B is stirred. Solution B is added drop by drop to solution A and it is stirred for 30 min.

Step 2: After stirring the precipitate was filtered.

Step 3: Then the precipitate was filtered by distilled water.

Step 4: After filtering with distilled water the precipitate was again washed by
. Hydrochloric acid and dried

Step 5: Then the precipitate was washed by acetone and dried.

Step 6: The sample obtained after drying the precipitate is powdered.

3.2 STRUCTURAL STUDIES

3.2.1 X-Ray Diffraction (XRD)

X-rays are electromagnetic radiation of wavelength about 1A° which is about the same size as an atom. X-ray Diffraction is a powerful nondestructive technique for characterizing the crystalline material. X-rays may be diffracted by passage through a crystal or by reflection (scattering) from a crystal, which consists of regular lattices of atom that serve as fine diffraction gratings. The resulting interference pattern may be photographed and analyzed to determine the wavelength of the incident X-ray or the spacing between the crystal atom, whichever is the unknown factor.

X-ray may also be diffracted by ruled gratings if the spacings are approximately equal to the wavelength of the incident x-ray. (1)

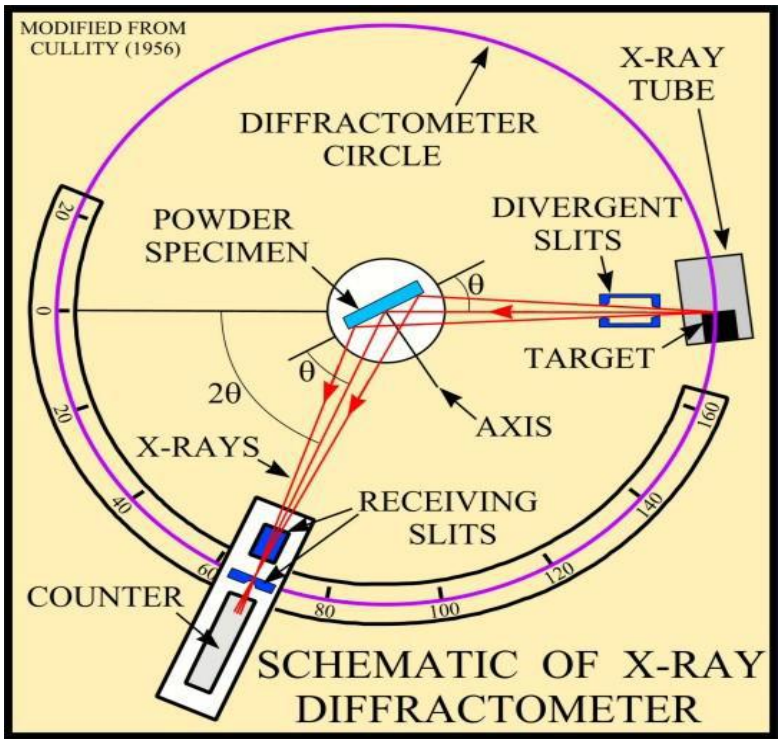

Fig 3.1 Schematic Diagram of X-ray Diffractometer

3.2.2 Principles of X-ray Diffraction

X-ray Diffraction (XRD) is a very important experimental technique that has been used for a long time to study the crystal structure of solids, lattice constants and geometry identification of unknown materials. XRD is a common technique for the study of crystal structures and atomic spacing. XRD is based on constructive and destructive interference should become observable when crystalline and molecular structures are exposed to x-rays.

3.2.3 Bragg's Formula

In XRD, a collimated beam of X-rays, with a wavelength typically ranging from 0.7 to 2 Å, is incident on a specimen and it is diffracted by the crystalline phases in the specimen according to Braggs law,

$$n\lambda = 2d \sin \theta$$

where, s

θ is the angle between the incident rays &the surface of the crystal.

N is contructive interference occurs when n is an integer (whole number).

d is the spacing between atomic planes in the crystalline phase and

λ is the X-ray wavelength.

The intensity of the diffracted X-ray is measured as a function of the diffraction angle 2θ and the specimen's orientation. This diffraction pattern is used to identify the specimen's crystalline phase. X-ray diffraction is a nondestructive testing and does not require elaborate sample preparation.

3.2.4 Scherrer's Formula

If there is no homogeneous strain, the crystallite size, D, can be estimated from the peak width with the Scherrer's formula,

$$\mathbf{D = k \lambda / \beta \cos \theta}$$

where,

λ is the x-ray wavelength

β is the full width of height maximum (FWHM) of a diffraction peak,

θ is the diffraction angle,

k is the Scherrer's constant of the order of unity.

In addition, X-ray diffraction only provides the collective information of the particle sizes and usually requires a sizeable amount of powder. This technique is very useful in characterizing nanoparticles. The film thickness of epitaxial and highly textured thin films can also be estimated with X-ray diffraction. (3)

3.2.5 Applications

XRD analysis has a wide range of applications in material science, chemistry, geology, environmental science, forensic science, and the pharmaceutical industry for characterizing materials. Amorphous materials are readily recognized by the absence of peaks in an XRD chart. The technique is also used for studying particles in liquid suspensions or polycrystalline solids (bulk or thin film materials). Other applications of

XRD analysis include determination of phase transitions in a given substance, semi-quantitative determination of phases present in a sample, measurement of crystallite size particularly in nano materials etc.(2)

3.3 FOURIER TRANFORM INFRARED SPECTROSCOPY

FTIR spectroscopy first developed by astronomers in the earth 1950s to study the infrared spectra of distant stars has now been developed into a very powerful technique for the detection of very weak signals from the environmental noise. It is a simple mathematical technique to resolve a complex wave into its frequency components. The conventional IR spectrometers are not of much use for the far IR region (20-400cm^{-1}) as the source are weak and detectors insensitive. FTIR has made this energy limited region more accessible. It has made the middle infrared (400-4000cm^{-1}).(5)

FT-IR Spectrometers are often simply called FTIRs. But for the purists, an FT-IR is a method of obtaining infrared spectra by first collecting an interferogram of a sample signal using an interferometer, and then performing a Fourier Transform (FT) on the interferogram to obtain the spectrum. An FT-IR Spectrometer collects and digitizes the interferogram, performs the FT function, and displays the spectrum. (4)

3.3.1 Working of FT-IR Spectrometer:

The Michelson Interferometer

A FT-IR is typically based on The Michelson Interferometer Experimental Setup. The interferometer consists of a beam splitter, a fixed mirror, and a mirror that translates back and forth, very precisely. The beam splitter is made of a special material that transmits half of the radiation striking it and reflects the other half. Radiation from the source strikes the beam splitter and separates into two beams. One beam is transmitted through the beam splitter to the fixed mirror and the second is reflected off the beam splitter to the moving mirror. The fixed and moving mirrors reflect the radiation back to the beam splitter. Again, half of this reflected radiation is transmitted and half is reflected at the beam splitter, resulting in one beam passing to the detector and the second back to the source. (4)

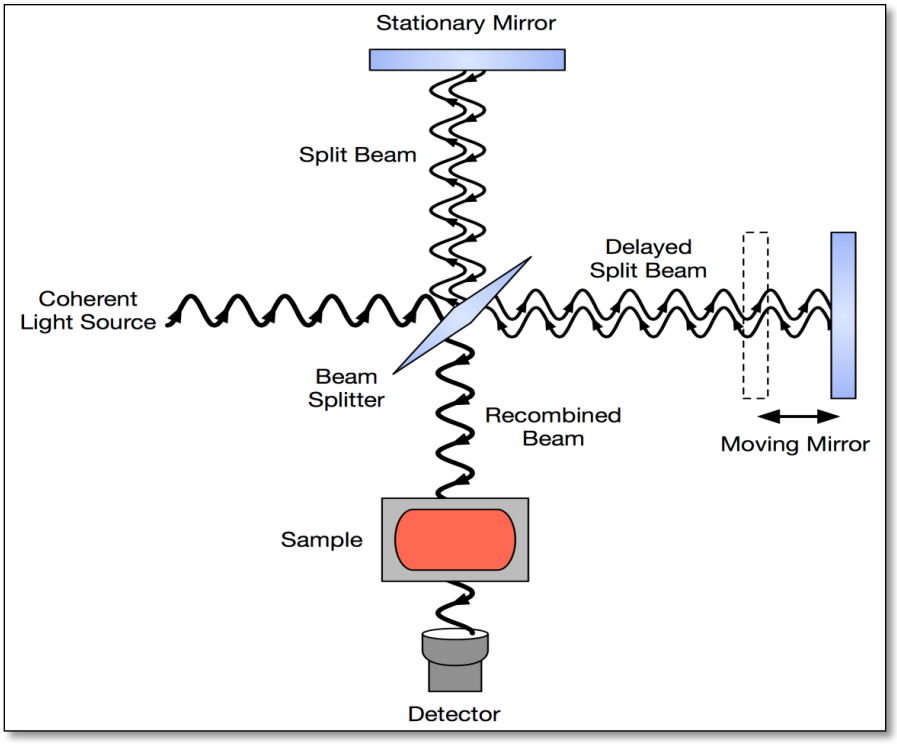

Fig 3.2 Schematic diagram of Michelson Interferometer

3.3.2 Application

FTIR can be used in all applications where a dispersive spectrometer was used in the past. Spectra can be measured in situations where very little energy reaches the detector and scan rates can exceed 50 spectra a second. An infrared microscope allows samples to be observed and spectra measured from regions as small as 5 microns across. Images can be generated by combining a microscope with linear or 2-D array detectors. The spatial resolution can approach 5 microns with tens of thousands of pixels. The images contain a spectrum for each pixel and can be viewed as maps showing the intensity at any wavelength or combination of wavelengths. This allows the distribution of different chemical species within the sample to be seen. Typical studies include analysing tissue sections as an alternative to conventional histopathology and examining the homogeneity of pharmaceutical tablets. (6)

3.4 ULTRAVIOLET- VISIBLE SPECTROSCPY

A large amount of energy is associated with ultraviolet radiation and hence the radiation is capable of including electronic excitation as well as rotational and vibrational transitions, also known as electronic spectroscopy. The UV visible spectrum is divided into three regions. Vacuum ultraviolet (10-200nm), near or quarts UV (200-280nm) in which the excitation of electron from p & d π – orbital of conjugated system occurs above 200nm and give rise to information spectra and visible region (400-750nm). As the organic molecule increases in conjugation of spectra fall in the visible region. On passing electromagnetic radiation in the UV and visible bonds, a portion of the radiation is normally absorbed by the compounds. The amount of absorption depends on the wavelength of the radiation and the structure of the compounds

3.4.1 Principle of UV spectroscopy

UV spectroscopy obeys the Beer-Lambert law, which states that, when a beam of monochromatic light is passed through a solution of an absorbing substance, the rate of decrease of intensity of radiation with thickness of the absorbing solution is proportional to the incident radiation as well as the concentration of the solution. The expression of Beer-Lambert law is

$$A = \log (I_0/I) = Ecl$$

Where,

A = absorbance

I_0 = intensity of light incident upon sample cell

I = intensity of light leaving sample cell

C = molar concentration of solute

L = length of sample cell (cm.)

E = molar absorptivity

From the Beer-Lambert law it is clear that greater the number of molecules capable of absorbing light of a given wavelength, the greater the extent of light absorption. This is the basic principle of UV spectroscopy.

3.4.2 Instrumentation and working of UV spectroscopy

Instrumentation and working of the UV spectrometers can be studied simultaneously. Most of the UV spectrometers consist of the following parts

Light Source: Tungsten filament lamps and Hydrogen-Deuterium lamps are most widely used and suitable light source as they cover the whole UV region. Tungsten filament lamps are rich in red radiations; more specifically they emit the radiations of 375 nm, while the intensity of Hydrogen-Deuterium lamps falls below 375 nm. **Monochromator**: Monochromators generally composed of prisms and slits. The most of the spectrophotometers are **double beam spectrophotometers**. The radiation emitted from the primary source is dispersed with the help of rotating prisms. The various wavelengths of the light source which are separated by the prism are then selected by the slits such the rotation of the prism results in a series of continuously increasing wavelength to pass through the slits for recording purpose. The beam selected by the slit is monochromatic and further divided into two beams with the help of another prism. **Sample and reference cells**: One of the two divided beams is passed through the sample solution and second beam is passé through the reference solution. Both sample and reference solution are contained in the cells. These cells are made of either silica or quartz. Glass can't be used for the cells as it also absorbs light in the UV region. **Detector**: Generally two photocells serve the purpose of detector in UV spectroscopy. One of the photocell receives the beam from sample cell and second detector receives the beam.

Amplifier: The alternating current generated in the photocells is transferred to the amplifier. The amplifier is coupled to a small servometer. Generally current generated in the photocells is of very low intensity, the main purpose of amplifier is to amplify the signals many times so that spectrum is obtained clear and recorded. (8)

3.5 PHOTOLUMINESCENCE

Photoluminescence spectroscopy is a contactless, nondestructive method of probing the electronic structure of materials. Light is directed onto a sample, where it is absorbed and imparts excess energy into the material in a process called photo-excitation. One way this excess energy can be dissipated through the emission of light by the sample and is called luminescence. In the case of photo-excitation, this luminescence is called photoluminescence.

Photo-excitation causes electrons within a material to move into permissible excited states. When these electrons return to their equilibrium states, the excess energy is released and may include the emission of light (a radiative process) or may not (a non-radiative process). The energy of the emitted light relates to the difference in energy levels between the two electron states involved in the transition between the excited state and the equilibrium state. The quantity of the emitted light is related to the relative contribution of the radiative process.

3.5.1 Forms of photoluminescence

Resonant radiation

In resonant radiation, a photon of a particular wavelength is absorbed and an equivalent photon is immediately emit, through which no significant internal energy transitions of the chemical substrate between absorption and emission are involved and the process is usually of an order of 10 nanoseconds.

Fluorescence

When the chemical substrate undergoes internal energy transitions before relaxing to its ground state by emitting photons, some of the absorbed energy is dissipated so that the emitted light photons are of lower energy than those absorbed. One of such most familiar phenomenon is fluorescence, which has a short lifetime (10^{-8} to 10^{-4} s).

Phosphorescence

Phosphorescence is a radiational transition, in which the absorbed energy undergoes intersystem crossing into a state with a different spin multiplicity. The lifetime of phosphorescence is usually from 10^{-4} - 10^{-2} s, much longer than that of Fluorescence. Therefore, phosphorescence is even rarer than fluorescence, since a molecule in the

triplet state has a good chance of undergoing intersystem crossing to ground state before phosphorescence can occur. (9)

3.6 Jablonski Diagram:

A Jablonski diagram is basically an energy diagram, arranged with energy on a vertical axis. The energy levels can be quantitatively denoted, but most of the diagrams use energy levels schematically. The rest of the diagram is arranged into columns. Every column usually represents a specific spin multiplicity for a particular species. However, some diagrams divide energy levels within the same spin multiplicity into different columns. Within each column, horizontal lines represent eigenstates for that particular molecule. Bold horizontal lines are representations of the limits of electronic energy states. Within each electronic energy state are multiple vibronic energy states that may be coupled with the electronic state. Usually only a portion of these vibrational eigenstates are represented due to the massive number of possible vibrations in a molecule. Each of these vibrational energy states can be subdivided even further into rotational energy levels; however, typical Jablonski diagrams omit such intense levels of detail. As electronic energy states increase, the difference in energy becomes continually less, eventually becoming a continuum that can be approach with classical mechanics. Additionally, as the electronic energy levels get closer together, the overlap of vibronic energy levels increases.

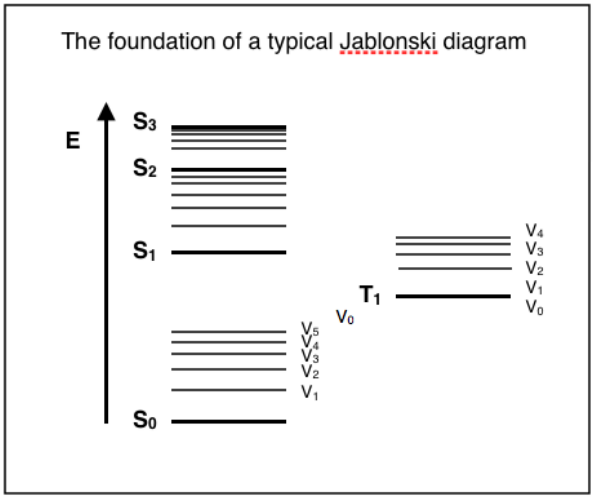

Fig 3.3 The foundation of a typical diagram

3.6.1 Absorbance

The first transition in most Jablonski diagrams is the absorbance of a photon of a particular energy by the molecule of interest. This is indicated by a straight arrow pointing up. Absorbance is the method by which an electron is excited from a lower energy level to a higher energy level. The energy of the photon is transferred to the particular electron. Those electron then transitions to a different eigenstate corresponding to the amount of energy transferred. Only certain wavelengths of light are possible for absorbance, that is, wavelengths that have energies that correspond to the energy difference between two different eigenstates of the particular molecule. Absorbance is a very fast transition, on the order of 10^{-15} seconds. Most Jablonski diagrams, however, do not indicate a time scale for the phenomenon being indicated. This transition will usually occur from the lowest (ground) electronic state due to the statistical mechanical issue of most electrons occupying a low lying state at reasonable temperatures. There is a Boltzmann distribution of electrons within this low lying levels, based on the the energy available to the molecules. This energy available is a function of the Boltzmann's constant and the temperature of the system. These low lying electrons will transition to an excited electronic state as well as some excited vibrational state.

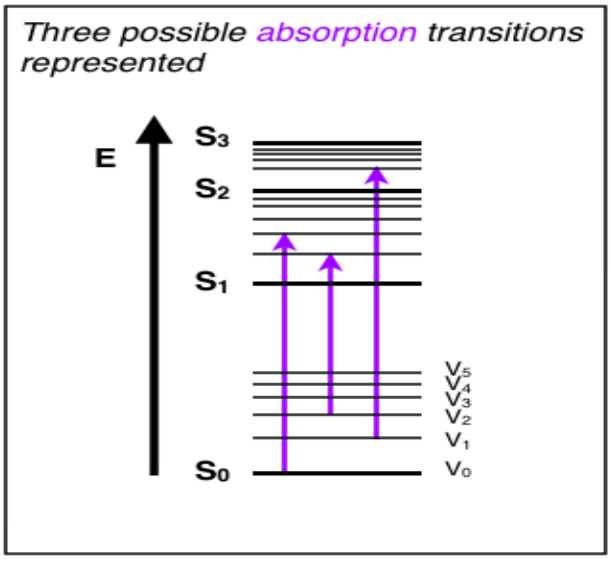

Fig 3.4 Three possible absorption transitions

3.6.2 Vibrational Relaxation and Internal Conversion

Once an electron is excited, there is a multitude of ways that energy may be dissipated. The first is through vibrational relaxation, a non-radiative process. This is indicated on the Jablonski diagram as a curved arrow between vibrational levels. Vibrational relaxation is where the energy deposited by the photon into the electron is given away to other vibrational modes as kinetic energy. This kinetic energy may stay within the same molecule, or it may be transferred to other molecules around the excited molecule, largely depending on the phase of the probed sample. This process is also very fast, between 10^{-14} and 10^{-11} seconds. Since this is a very fast transition, it is extremely likely to occur immediately following absorbance. This relaxation occurs between vibrational levels, so generally electrons will not change from one electronic level to another through this method.

However, if vibrational energy levels strongly overlap electronic energy levels, a possibility exists that the excited electron can transition from a vibration level in one electronic state to another vibration level in a lower electronic state. This process is called internal conversion and mechanistically is identical to vibrational relaxation. It is also indicated as a curved line on a Jablonski diagram, between two vibrational levels in different electronic states. Internal Conversion occurs because of the overlap of vibration and electronic energy states. As energies increase, the manifold of vibrational and electronic eigenstates becomes ever closer distributed. At energy levels greater than the first excited state, the manifold of vibrational energy levels strongly overlaps with the electronic levels. This overlap gives a higher degree of probability that the electron can transition between vibrational levels that will lower the electronic state. Internal conversion occurs in the same time frame as vibrational relaxation, therefore, is a very likely way for molecules to dissipate energy from light perturbation. However, due to a lack of vibrational and electronic energy state overlap and a large energy difference between the ground state and first excited state, internal conversion is very slow for an electron to return to the ground state. This slow return to the ground state lets other transitive processes compete with internal conversion at the first electronically excited

state. Both vibrational relaxation and internal conversion occur in most perturbations, yet are seldom the final transition.

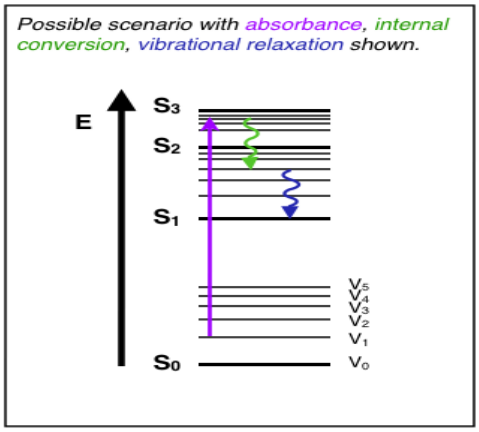

Fig 3.5 shows that possible scenario with absorbance, internal conversion, vibrational relaxation

3.6.3 Fluorescence

Another pathway for molecules to deal with energy received from photons is to emit a photon. This is termed fluorescence. It is indicated on a Jablonski diagram as a straight line going down on the energy axis between electronic states. Fluorescence is a slow process on the order of 10-9 to 10-7 seconds; therefore, it is not a very likely path for an electron to dissipate energy especially at electronic energy states higher than the first excited state. While this transition is slow, it is an allowed transition with the electron staying in the same multiplicity manifold. Fluorescence is most often observed between the first excited electron state and the ground state for any particular molecule because at higher energies it is more likely that energy will be dissipated through internal conversion and vibrational relaxation. At the first excited state, fluorescence can compete in regard to timescales with other non-radiative processes. The energy of the photon emitted in fluorescence is the same energy as the difference between the eigenstates of the transition; however, the energy of fluorescent photons is always less than that of the exciting photons. This difference is because energy is lost in internal conversion and vibrational relaxation, where it is transferred away from the electron. Due to the large

number of vibrational levels that can be coupled into the transition between electronic states, measured emission is usually distributed over a range of wavelengths.

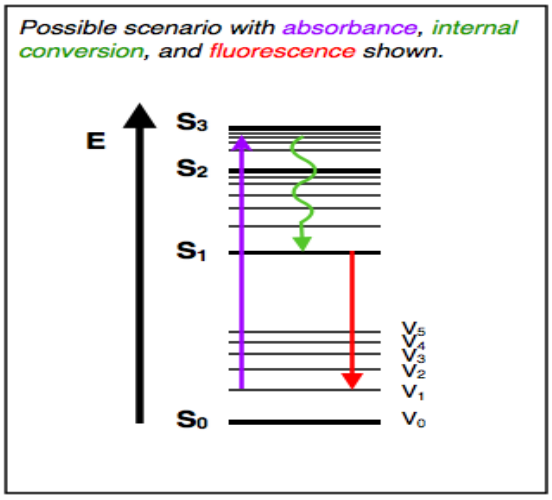

Fig 3.6 possible scenario with absorbance, internal conversion, fluorescence

3.6.4 Intersystem Crossing

Yet another path a molecule may take in the dissipation of energy is called intersystem crossing. The electron changes spin multiplicity from an excited singlet state to an excited triplet state. It is indicated by a horizontal, curved arrow from one column to another. This is the slowest process in the Jablonski diagram, several orders of magnitude slower than fluorescence. This slow transition is a forbidden transition, that is, a transition that based strictly on electronic selection rules should not happen. However, by coupling vibrational factors into the selection rules, the transition becomes weakly allowed and able to compete with the time scale of fluorescence. Intersystem crossing leads to several interesting routes back to the ground electronic state. One direct transition is phosphorescence, where a radiative transition from an excited triplet state to a singlet ground state occurs. This is also a very slow, forbidden transition. Another possibility is delayed fluorescence, the transition back to the first excited singlet level, leading to the emitting transition to the ground electronic state.

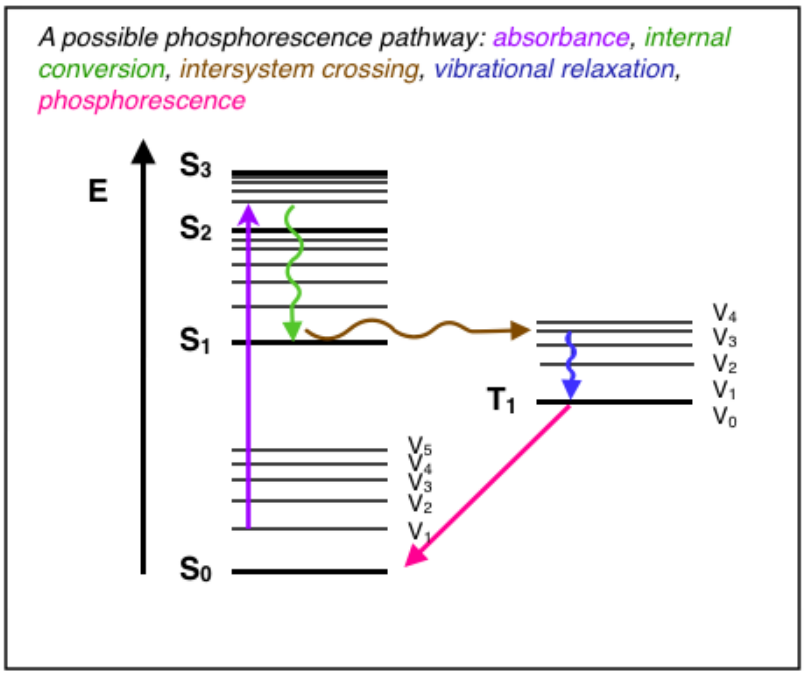

Fig 3.7 Possible phosphorescence pathway: absorbance, internal conversion, intersystem crossing, vibrational relaxation, phosphorescence

3.6.5 Time Scale

It is important to note that a Jablonski diagram shows what sorts of transitions that can possibly happen in a particular molecule. Each of these possibilities is dependent on the time scales of each transition. The faster the transition, the more likely it is to happen as determined by selection rules. Therefore, understanding the time scales each process can happen is imperative to understanding if the process may happen.

Each process outlined above can be combined into a single Jablonski diagram for a particular molecule to give a overall picture of possible results of perturbation of a molecule by light energy. Jablonski diagrams are used to easily visualize the complex inner workings of how electrons change eigenstates in different conditions. Through this simple model, specific quantum mechanical phenomena are easily communicated. (9) (10)

REFERENCE

1. Arul Solanki, spectroscopy; oxford Book Company; first edition (2009), pg 78-79.
2. https://www.researchgate.net/publication/260659249_X-ray Diffraction Analysis Principle_Instrument_and Applications
3. A.Segmuller and M.Murakami; in thin films from free atoms and particles, ed K.J.Klabunde; Academic Press, Orlando, FL; 325; 1985.
4. http://www.newport.com/Introduction-to-FTIR-Spectroscopy/405840/1033/content.aspx
5. Aruldhas.G, Molecular structure and spectroscopy: published by Asoke k.Glosh: prentice hall of India private limited, sixth edition October (2005). pg 195
6. https://en.wikipedia.org/wiki/Fourier_transform_infrared_spectroscopy#Applications
7. http://www.indiastudychannel.com/resources/146681-Principle-working-and-applications-of-UV-spectroscopy.aspx
8. http://cnx.org/contents/gbsDEZju@2/Photoluminescence-Spectroscopy.
9. H. H. Jaffe and Albert L. Miller "The fates of electronic excitation energy" J. Chem. Educ., 1966, 43 (9), pg 469
10. E. B. Priestley and A. Haug "Phosphorescence Spectrum of Pure Crystalline Naphthalene" J. Chem. Phys. 49, 622 (1968),

CHAPTER-IV

RESULTS AND DISCUSSION

4.1 INTRODUCTION:

Structural and phase analysis, morphological, vibrational and optical properties of tin antimony and Terbium doped tin antimony nanoparticles are analysed by X-ray diffraction, FTIR, UV-Vis spectra and Photoluminescence analysis. The obtained results are discussed in this chapter.

4.2 Structural Characterization

4.2.1 X-Ray Diffraction Analysis (XRD)

The prepared Sn_2Sb_3 and $Sn_{1.4}Tb_{0.6}Sb_3$ composition doped with Terbium is investigated with X-ray Diffraction to determine the phase formation. The X-Ray diffraction pattern of SnSb doped with terbium compositions as prepared by co-precipitation method is shown in Figure 4.1. The Sn_2Sb_3in the composition 2:3 is doped with three compositions namely 0.2, 0.4 and 0.6 of Tb in this host lattice. The results observed for 0.6 is the best and only this composition results are presented here. In all the samples, the peaks at 28^0,41^0,42^0,51^0 and 60^0 corresponds to the (101), (012), (110), (003), and (202) for Sn_2Sb_3.

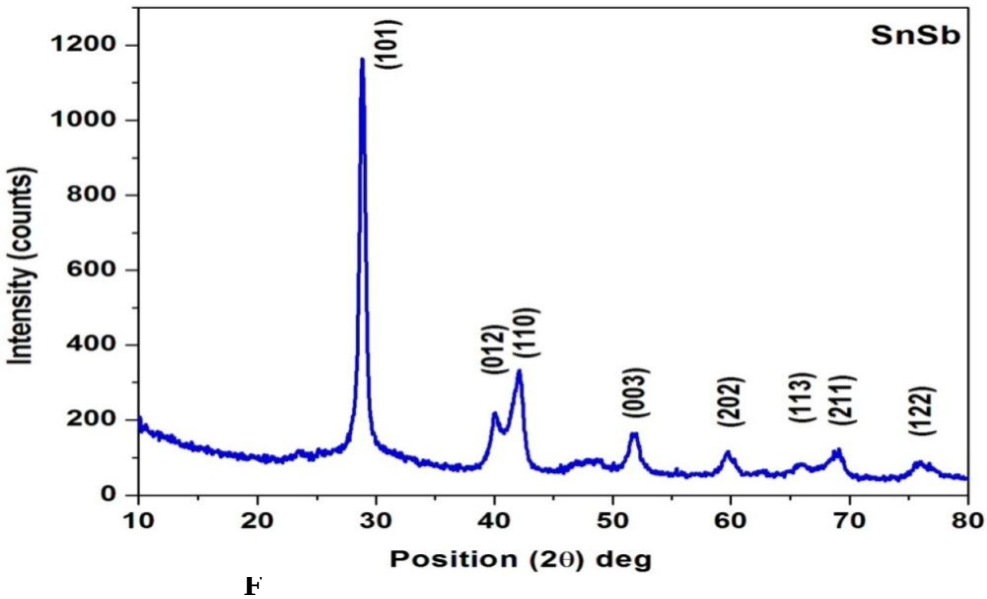

F

Figure 4.1 X-ray Diffractogram of the Sn_2Sb_3 alloy

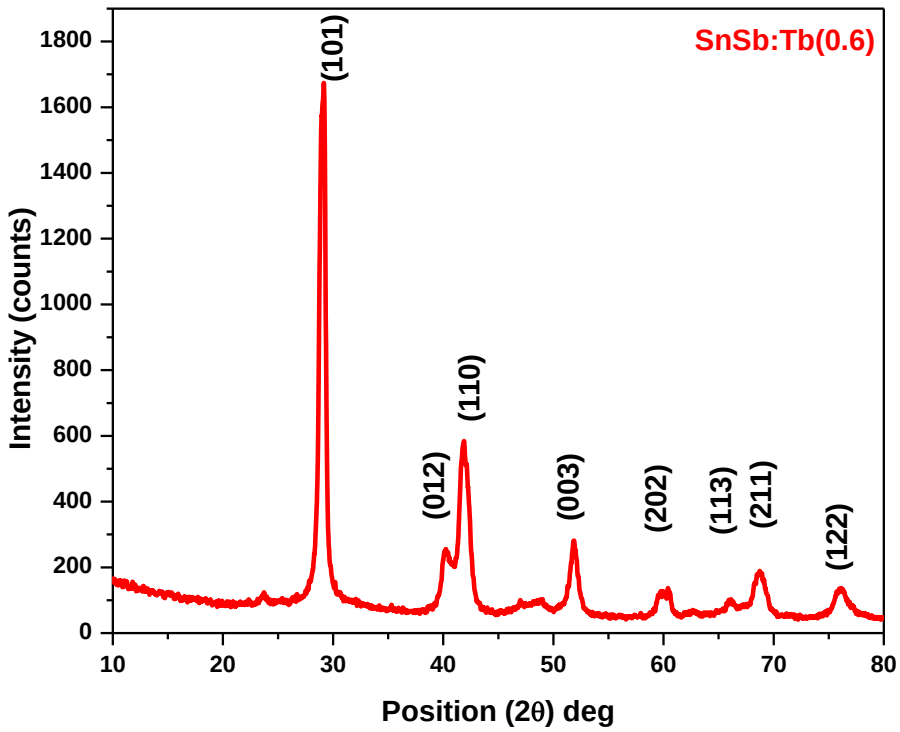

Figure 4.2 X-ray diffractogram of the $Sn_{1.4}Tb_{0.6}Sb_3$

A sharp peak obtained in XRD pattern indicates the crystallinity of the prepared samples. The XRD pattern observed for $Sn_{1.4}Tb_{0.6}Sb_3$ is not different from that of the Sn_2Sb_3. This indicates that the structure is left undisturbed by the cerium atoms in the substitution limits which are chosen in these studies. It is also to be noted that there are no new peaks observed in doped sample which is an indication of the stable crystal structure for the doped Sn_2Sb_3. The results are analyzed with the standard diffraction pattern (JCPDS card no- 33-0118) and the crystal system possesses rhombohedral structure. Due the fact that all the peaks except one at 68˚ which is assigned as (004) peak falls into the formula –h+k+l=3n which is for a hexagonal structure. Hence the structure has got rhombohedral structure falling into irregular hexagonal distribution of atoms. The lattice parameter calculated is given in the Table 4.1. Compared to the JCPDS lattice parameters, there is a size reduction in "c" when "a" is maintained and when "a" is reduced "c" is blotted. But, it is to be noted that this size variation is just few 100^{th} is an angstrom and is not of much importance. The similar behavior is observed for the doped Sn_2Sb_3. All the remaining peaks are assigned to the corresponding (hkl) planes

based on the JCPDS data as indicated in the figure 4.1 and 4.2 respectively. Crystallite size is calculated by using Debye Scherrer formula

$$d = 0.9\lambda / \beta\cos(\theta)$$

where,

d is the Crystallite size,

λ is the wavelength of the radiation (1.5405Å for Cu-Kα radiation),

β is the full width at half maximum of the peak (radians),

θ is half of the peak position (radians).

The diffraction peaks observed at 28.75^0, 40.04^0, 42.11^0, 51.87^0, 59.64^0, 66.01^0, and 68.95^0 shows a small shift in position towards the higher angle side in the doped sample compared to the undoped sample which is an indication of either the crystallite size increment and increased strain in the doped Sn_2Sb_3. Lattice strain value of both the samples were calculated using the formula,

$$\varepsilon = \beta \cot(\theta)$$

where

ε - Strain

β-Full width at half maximum of the peak (radians)

θ- half of the peak position

The calculated values of crystallite size, lattice strain and all the other lattice parameters obtained for both the samples are listed in the table 4.1 and 4.2. The increment in crystallite size is observed for $Sn_{1.4}Tb_{0.6}Sb_3$ sample from 16 nm to 21 nm. This may be due to the higher ionic radius of terbium (Ionic radii: Tb-0.923Å; Sn-0.55 Å; Sb- 0.76 Å)

Table 4.1 The different <hkl> planes assignment to the XRD peaks obtained Sn_2Sb_3; lattice constants, a= 4.428Å, c= 5.2886Å, Volume = 89.797 Å3

No .of peaks	2θ (deg)	H	K	L	$1/d^2$ cal ($x10^8$)	FWHM	Strain
1	23.626	1	0	1	2.451	0.802	0.002
2	28.757	0	1	2	2.105	0.334	0.005
3	40.042	1	1	0	3.181	0.401	0.007
4	42.110	0	0	3	1.320	0.267	0.004
5	51.871	2	0	2	1.140	0.669	0.011
6	59.646	1	1	3	1.179	0.802	0.014
7	66.010	2	1	1	1.028	0.802	0.014
8	68.959	1	2	2	2.451	0.936	0.016

Table 4.2 The different <hkl> planes assignment to the XRD peaks obtained $Sn_{1.4}Tb_{0.6}Sb_3$; lattice constants, a= 3.37Å, c= 5.289Å, Volume = 86.095 $Å^3$

Peak no	2θ	H	K	L	$(1/d^2)$	FWHM	Strain
1	28.93	1	0	1	3.505	0.234	0.010
2	40.03	0	1	2	1.579	0.535	0.003
3	41.81	1	1	0	1.588	0.535	0.032
4	51.85	0	0	3	1.885	0.468	0.034
5	68.81	2	1	1	2.055	0.468	0.004

4.3 Optical Characterization

4.3.1 Fourier Transform Infrared Analysis (FTIR)

FTIR spectra of Sn_2Sb_3 and $Sn_{1.4}Tb_{0.6}Sb_3$ powder are recorded at room temperature in the wavelength range of 4000- 400 cm^{-1}. Few peaks are observed have changed while doping terbium when compared to the undoped. In $Sn_{1.4}Tb_{0.6}Sb_3$, new peak has arisen at 1708.67 cm^{-1}, 1215.05 cm^{-1}, 540.40 cm^{-1}, 486.72 cm^{-1} which may be attributed to the incorporation of terbium in the lattice.

The range of vibrations obtained in the region of 3000 cm^{-1} is attributed to the OH vibrations which may be due to the moisture content due to the hygroscopicity of KBr during the pelletization. The various peaks observed in the recorded region are assigned to the intermetallic bonds (1). The vibrations between 500 and 700cm-1 observed in the undoped sample is subdued in the terbium doped sample indicating the curtailment of freedom of oscillation by the dopant in the lattice. Comparing the FTIR spectrum to the oxides of the Sn, Sb and Tb from the literature, it can be ascertained that the samples are free from oxide impurities. The obtained vibrational peaks and the corresponding shift in wave numbers for terbium doped Sn_2Sb_3 are listed in the Table 4.3.

Table 4.3 Vibrational peaks assignment for Sn_2Sb_3 and $Sn_{1.4}Tb_{0.6}Sb_3$ samples

Peak no	Sn_2Sb_3	$Sn_{1.4}Tb_{0.6}Sb_3$	Peak
1	-	486.67	After addition of Tb
2	586.62	540.43	Sn-Sb
3	671.25	-	Disappeared after addition of Tb
4	746.55	-	
5	1015.71	1359.57	Sn-Sb
6	1654.82	1626.66	OH vibration
7	2327.85	-	Sn-Sb
8	2369.82	-	
9	2924.92	2922.59	Impurities from acetone
10	-	3403.74	OH vibration

Altogether, it is clear that Tb has entered into the crystal structure and bonded with Sn/Sb. However, the rhombohedral structure is unaltered and this statement is validated in comparison with the XRD pattern observed for both the samples

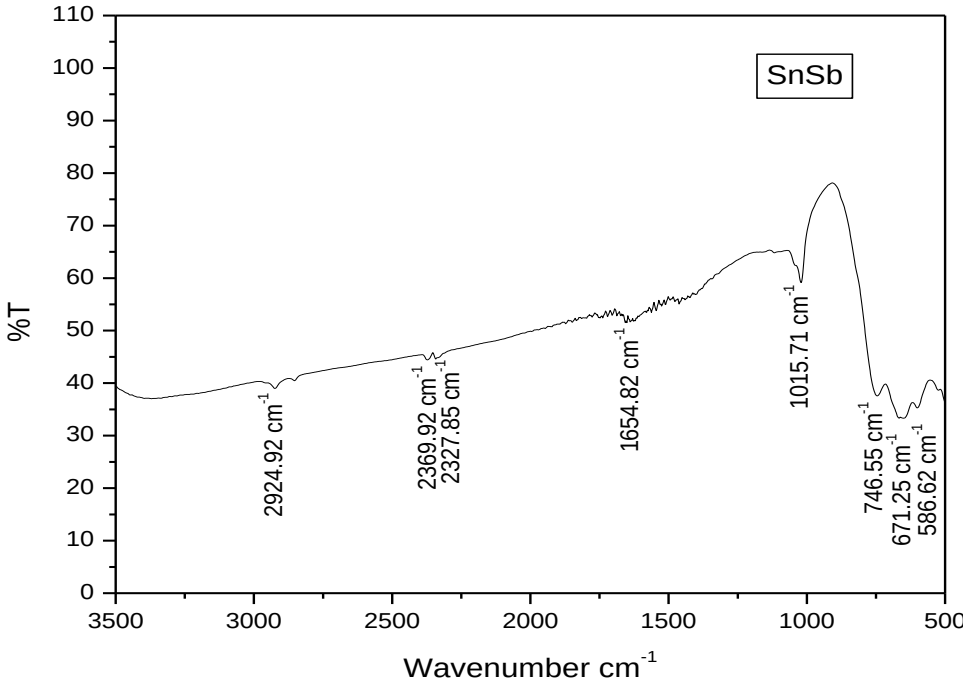

Fig 4.3: FTIR spectrum of Sn_2Sb_3

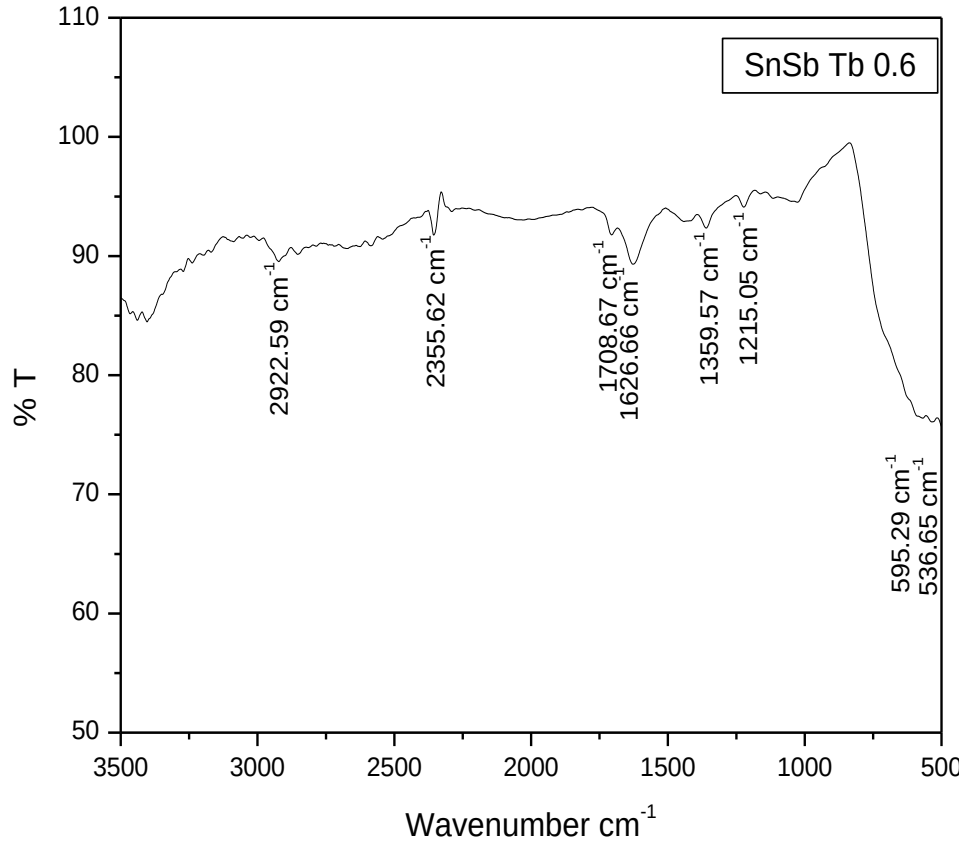

Fig 4.4: FTIR spectrum of $Sn_{1.4}Tb_{0.6}Sb_3$

4.3.2 Electronic Structure analysis:

The electronic structure of the samples could be explored by the absorption and emission studies. Hence Uv-Vis –Nir spectra and Photoluminescence spectra were analysed.

4.3.3 UV Visible analysis

The UV-Vis-NIR analysis of material is performed on using Jasco V600 spectrophotometer. Fig 4.5 shows the UV-Vis-NIR absorption spectrum of SnSb doped terbium. It is found that a broad absorption is observed from 400 to 700 in this material which is very much favorable for any lighting applications. A very good profile of IR absorption is also very much favorable in this material.

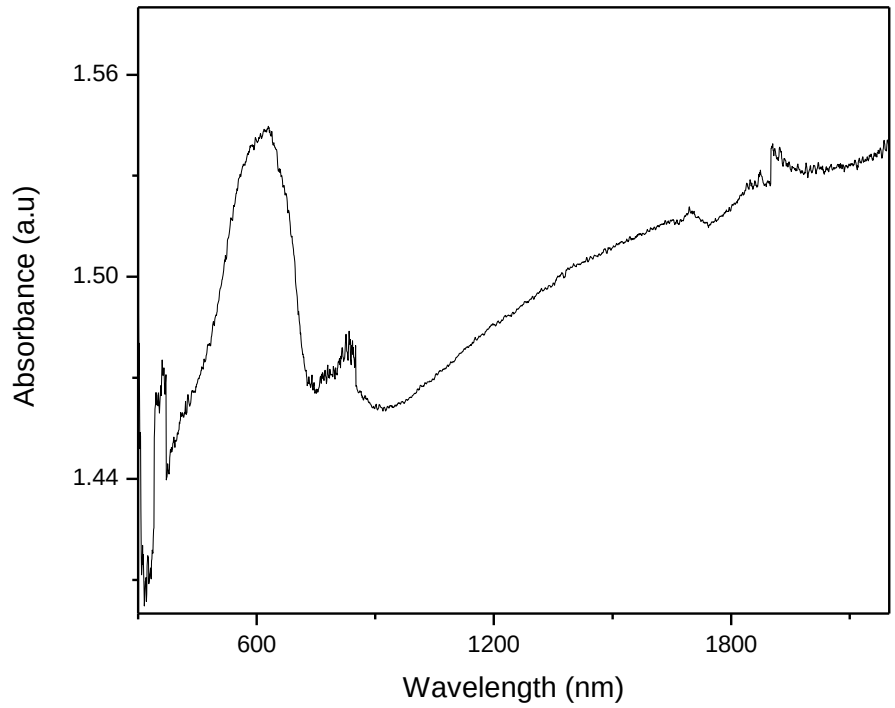

Figure.4.5 Absorption spectrum of $Sn_{1.4}Tb_{0.6}Sb_3$

The tauc plot, with $(\alpha h\nu)^2$ vs $h\nu$, is shown in Figure 4.7 and analysed for understanding the electronic structure of the sample. A band gap of 2.03 eV is observed with the band edges, the HOMO and LUMO levels at 1.52 eV and 3.55eV. The S_0 band and S_1 band could be observed clearly that is shown in Figure 4.6.

The lower energy of the tauc plot is further analysed and it is seen that the band gap that had existed from nearly 1.4eV to 1.3eV in the host lattice has been completely filled due to the substitution of terbium in the SnSb lattice. This is shown in Figure 4.7. Thus the electronic band structure is analysed and the emission profile of this material is analysed using photoluminescence technique and is the results are presented here.

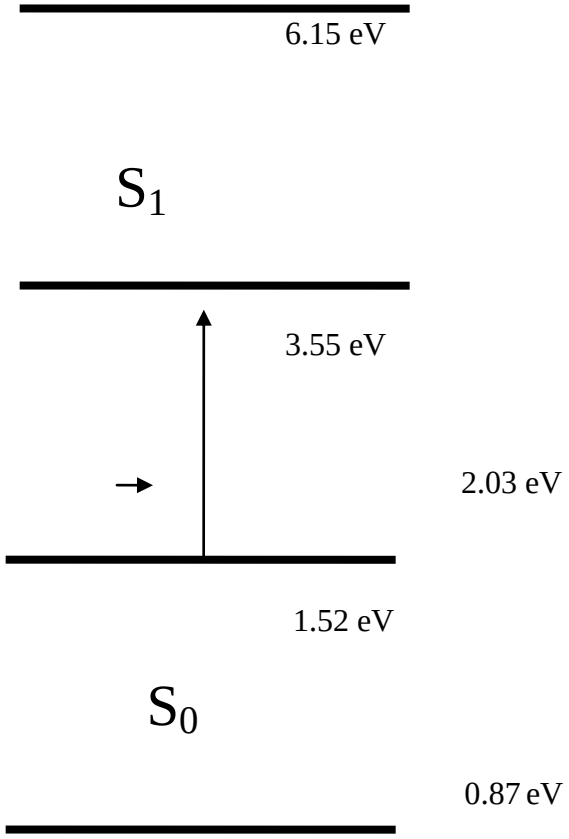

Fig 4.6 Energy band diagram of $Sn_{1.4}Tb_{0.6}Sb_3$

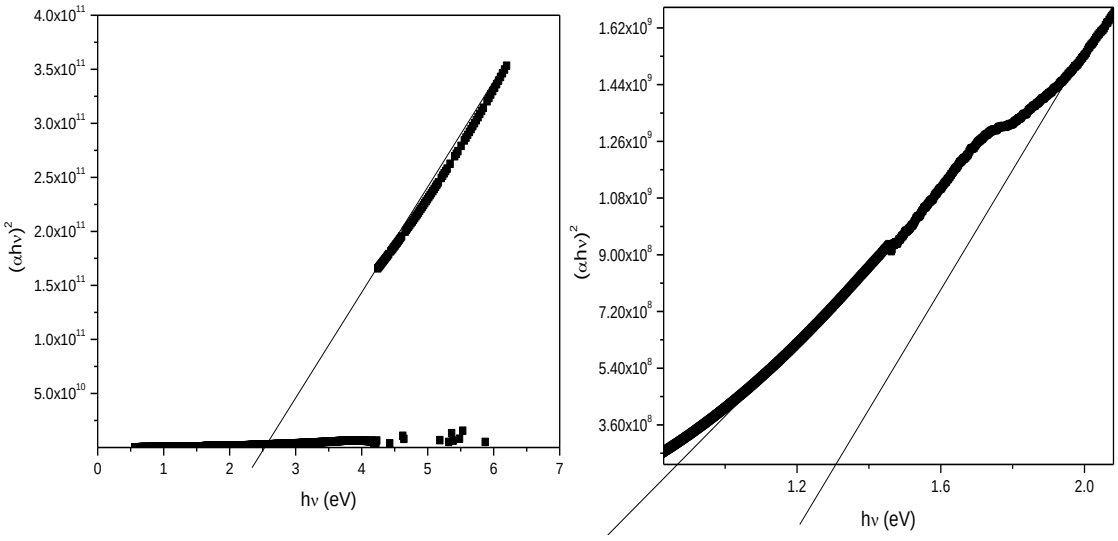

Fig 4.7 UV visible spectrum of $Sn_{1.4}Tb_{0.6}Sb_3$

4.3.4 Photoluminescence (PL)

The energy gap (Eg) is an important feature of semiconductors which determines their applications in optoelectronics. This wide band gap can be altered if the particle size of the system lies in the nanometric region. The large band gap coupled with its large excitonic binding energy has made it a potential candidate in light emitting diodes

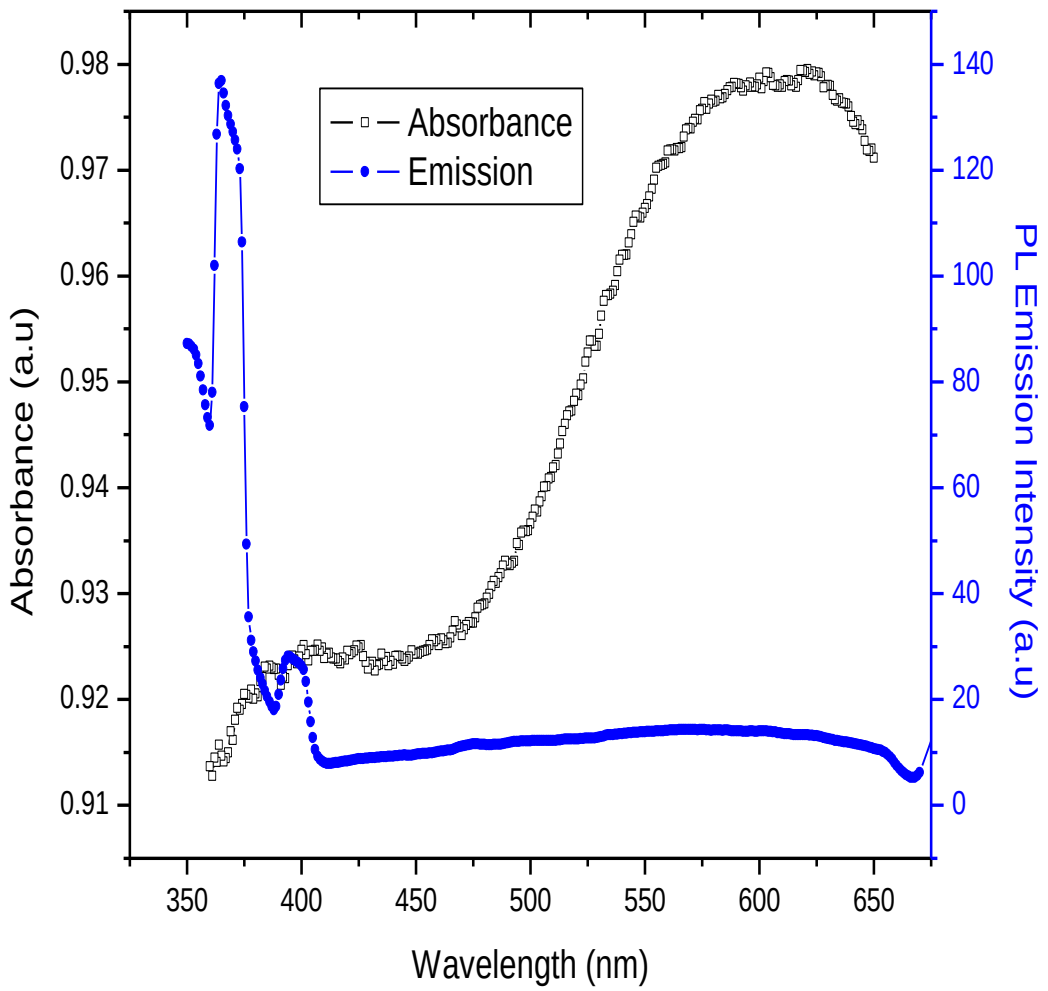

Fig 4.8 Absorption and Emission spectrum of $Sn_{1.4}Tb_{0.6}Sb_3$

Figure 4.8 shows the absorption and emission of the $Sn_{1.4}Tb_{0.6}Sb_3$ and the salient feature observed in this profile is that the emission at 400nm is corroborated with an absorption indicating that this could act as a direct band gap material.

REFERENCE

1. P. Nithyadharseni, B. Nalini, P. Saravanan, Applied Surface Science 311 (2014) 503–507
2. László Kőrösi, Szilvia Papp, Imre Dékány, Thin Solid Films 519 (2011) 3113–3118
3. J. Kaspar, P. Fornasiero, G.Balducci, R. Di Monte, N. Hickey, V. Sergo, Efect of SnSb content on textural and structural properties of solid solutions made by citrate complexation route, Inorganic ChimicaActa, Volume- 349, 2003, pages: 217-226.
4. Yu Muto, Nobuto Oka, Naoki Tsukamoto, Yoshinori Iwabuchi, Hidefumi Kotsubo, Yuzo Shigesato, High-rate deposition of Sb-doped SnO_2 films by reactive sputtering using the impedance control method, Thin Solid Films, Volume 520, Issue 4, 1 December 2011, Pages: 1165-1366

CHAPTER V

SUMMARY AND CONCLUSION

Incorporation of terbium in the SnSb host is done by coprecipitation. Phase has been confirmed using XRD. The phase is confirmed to be rhombohedral. The absence of oxide formation is confirmed by FTIR and the incorporation of Terbium in this lattice binds the Sn or Sb thus some of the vibrational frequencies are not present. Absorption spectrum of the sample shows a wide absorption in the visible region qualifying this material for any lighting applications. Also the analysis of the electronic transition indicates that this could be a prospective direct band gap at 3.09eV in this material.